

Parametric PerceptNet: A bio-inspired deep-net trained for Image Quality Assessment

Jorge Vila-Tomás¹, Pablo Hernández-Cámara¹, Valero Laparra¹, Jesús Malo¹
¹*Image Processing Lab, Universitat de València, Paterna, 46980, Spain*

Abstract—Human vision models are at the core of image processing. For instance, classical approaches to the problem of image quality are based on models that include knowledge about human vision. However, nowadays, deep learning approaches have obtained competitive results by simply approaching this problem as regression of human decisions, and training a standard network on human-rated datasets. These approaches have the advantages of being easily adaptable to a particular problem and they fit very efficiently when data is available. However, mainly due to the excess of parameters, they have the problems of lack of interpretability, and over-fitting.

Here we propose a vision model that combines the best of both worlds by using a parametric neural network architecture. We parameterize the layers to have biplausible functionality, and provide a set of biplausible parameters.

We analyzed different versions of the model and compared it with the non-parametric version. The parametric models achieve a three orders of magnitude reduction in the number of parameters without suffering in regression performance. Furthermore, we show that the parametric models behave better during training and are easier to interpret as vision models. Interestingly, we find that, even initialized with biplausible parameters, the models diverge from biplausible solutions when trained for regression using human-rated datasets, which we call the *feature-spreading problem*. This suggests that the deep learning approach is inherently flawed, and emphasizes the need to evaluate and train models beyond regression.

Index Terms—Image Quality Metrics, Human Vision, Parametric Neural Networks

I. INTRODUCTION

The traditional methodology to tackle an image processing problem has been based on vision science. Either directly using vision models or relying on human perceptual knowledge, but also indirectly, such as scene statistics or even practical approaches based on human heuristic behavior. In particular, the problem of describing the quality of an image lends itself well to be approached from the point of view of vision science, since the quality of an image is usually qualified by a human observer. For instance, the Contrast Sensitivity Functions (CSFs) [1], [2] (which are equivalent to the application of layers of center-surround neurons [3]–[6]) were proposed to be considered for image quality assessment in the 70’s [7] shortly after the definition of the CSFs in the 60’s. Opponent chromatic channels [4], [8] together with Gabor-like filter-banks [9]–[13] and simple masking nonlinearities were proposed to be used together in measuring image distortions [14]. These simplified (point-wise) masking nonlinearities of *visual neuroscience* [15]–[17] are similar to the sigmoid activation functions of the *artificial neural networks* (ANNs) community [18], [19]. Variants of these simplified

(fixed) nonlinearities dominated the image quality scene in the 80’s and early 90’s [20]–[23]. However, in *vision science* as opposed to conventional activation sigmoids in ANNs, these nonlinearities are known to be adaptive instead of fixed [11], [24], [24]–[27]. This adaptive behavior is rooted in classical models of *visual neuroscience*, either recurrent [28]–[30] or feed-forward such as the Divisive Normalization (DN) [31]–[35]. These recurrent or normalization models (which have been shown to be equivalent [36], [37]) were successfully included in image/video quality too through the DN [38]–[44].

On the other hand, the Barlow hypothesis that tries to explain the organization of the visual system based on *unsupervised learning* [45], [46], fueled approaches for subjective quality based on image statistics in the first decade of this century. For instance, visual similarity was related to the preservation of image statistics in the spatial domain [47], [48] or in transform domains [49], [50] and following [51], metrics based on DN [42], [43] were interpreted to be implementing density factorization by capturing the structure of natural images in wavelet domains [52], [53]. Also in a statistical vein, visual fidelity was related to information flow in noisy-wavelet models of early vision [54], [55], and advances can be done by improving the information treatment of the model [56]–[58].

For more than 40 years, the above (interpretable models with a small number of parameters) were hand-crafted using a lot of prior biological and statistical knowledge. Interestingly, this paradigm started to change with the advent of easy-to-use automatic differentiation frameworks in the 2010’s. One of the first examples of this new trend was the metric proposed in [44]. This metric was still attached to a biologically sensible and simple linear+DN model, but was end-to-end optimized to maximize the correlation with an image quality database, which is one of the usual approaches today [59]. Regardless of the task for which the deep-learning distortion metrics have been trained for [60]–[62], the common ground of the current state-of-the-art metrics is their complexity compared to the simplicity of [44], or other (relatively shallow) nonparametric distance measure which also includes the biologically-inspired end-to-end optimized DNs: *the PerceptNet* [63].

As nowadays is very easy to find powerful regression tools, some people think that this problem is fully understood since it could be reduced to maximize the correlation with a subjectively rated database [64]. However, this naive view may not be true [65]. We argue that the complexity (or absence of biological/statistical constraints) is an intrinsic problem of the deep learning based models. Networks with millions of parameters necessarily have robustness and generalization problems that are well known by the deep learning community. For

instance, a deep learning method, LPIPS, does not outperform classical models in classical human-rated databases [60]. More importantly, conventional nonparametric deep metrics such as LPIPS or the original PerceptNet are hardly interpretable as vision models. For instance, it is hard to interpret the model features because these are spread along the layers of the nets in non-trivial ways. Preliminary evidences of that this *feature-spreading* problem is critical were presented in conferences [66]–[68]. A related problem is that detection thresholds of sensible visual features in conventional deep-perceptual metrics are far from human [69]. In fact, Goodfellow et al. motivates the introduction of *batch normalization* with this lateral comment [19]:

“Very deep models involve the composition of several functions, or layers. The gradient tells how to update each parameter, under the assumption that the other layers do not change. In practice, we update all the layers simultaneously. When we make the update, unexpected results can happen because many functions composed together are changed simultaneously, using updates that were computed under the assumption that the other functions remain constant.”

The intuition about this undesirable phenomenon is a very clever motivation of *batch normalization*: when using ReLUs the introduction of additional nonlinearities between linear layers certainly alleviates the mentioned parameter redundancy problem.

In this paper, we propose a model that has the principles of vision science at its roots, but has been designed from the point of view of the deep learning paradigm. In particular, we propose a parametric neural network that can be viewed as a vision model. The functionality and default parameters of each of the layers are bioinspired. The network has 3 orders of magnitude fewer parameters than the nonparametric version, behaves better during training, its features can be easily interpreted, and it has similar performance in regression tasks. The model is based on a nonparametric approach, the *PerceptNet* [63], because it was designed with the appropriate number of layers to accommodate the different known vision facts in the retina-V1 pathway. Moreover, it is equipped with bioinspired DN activations. From that, we parametrize *all* the layers, dramatically reducing the model complexity. This new setting allows an exploration that has not been done before: we study how, after initializing the parametric model with biologically plausible values, subsequent optimization can result in either biologically faithful or divergent outcomes, depending on the degree of constraint imposed, and we can always compare with the unconstrained (nonparametric) baseline. This opens new avenues for evaluating how closely such models align with human visual behavior and the need for novel evaluation metrics beyond traditional benchmarks.

The structure of the work is as follows: Section II sketches the general structure of the *Parametric PerceptNet*, and shows a motivating example that illustrates the positive bias induced by the parametrization. Section III addresses the conceptual difference between parametric and nonparametric models in

the training, and goes into the specific expressions of the layers. After that we describe the data (sec. IV) to be used in the experimental Section (sec. V) where we show different results. First, we analyze the effect of the bioinspired layers and the provided default parameters. We compare the behavior during training of the parametric and the nonparametric models. We analyze further three specific versions of the model in vision science terms. Section VI discusses the reasons for the observed behaviors and the implications in the context of related work, and finally Section VII concludes the paper.

II. SKETCH OF THE PARAMETRIC PERCEPTNET

The general structure of the proposed model, the *Parametric PerceptNet*, is illustrated in Fig. 1. Although fairly standard from the vision science perspective (recent models such as [35], [37], [44], [57], [65], [83], [84] have similar structure and physically/psychophysically calibrated flavor), the important point from the technical perspective is that *its architecture is completely comparable* to the previously reported end-to-end optimized nonparametric *PerceptNet* [63]. The original *PerceptNet* is a fair illustration of the current approach to build image quality metrics using deep networks. Note that it is very similar to Alexnet [85] and VGG models [86] in the sense of being a relatively shallow, feed-forward net with progressive reduction of resolution and increase of feature channels. However, *PerceptNet* has a crucial *biological* difference with those: the use of Divisive Normalization (DN) as activation function. In fact, DN is absent in VGG and but kind of implemented in Alexnet. What Krizhevsky et al. call as local normalization of features (a form of DN) is ignored in many on-line-available versions of Alexnet despite the authors mention that it is the second more important factor of its performance after ReLU [85]. In this regard, there are several reports [35], [87]–[91] that propose DNs as more biologically inspired than the one presented in [85].

In contrast, the proposed *Parametric PerceptNet* has a *crucial difference* with regard to the original (nonparametric) *PerceptNet*: instead of using unconstrained kernels (both in the linear layers and in the DNs), here we enforce each layer to perform the mathematical operation it is expected to do from a biological point of view. To do so we define a parametric (functional) form for each layer (sec III-B). This will allow us to propose a set of bioinspired parameters. On the other hand, we will check also the effect of fitting the model parameters to maximize the alignment with subjectively rated image quality databases (as in the case of the original *Perceptnet* or LPIPS). Training a parametric model has some specifics to take into account described in section III-A.

A. Motivating example

Before going into the necessary details of the implementation of the proposed *Parametric PerceptNet*, we illustrate the positive bias the parametrization induces. We follow the conventional evaluation of image/video quality metrics (sec. IV). In particular, we compare the Pearson correlations obtained by multiple random initializations, without further training, of the nonparametric *PerceptNet* and the proposed parametric

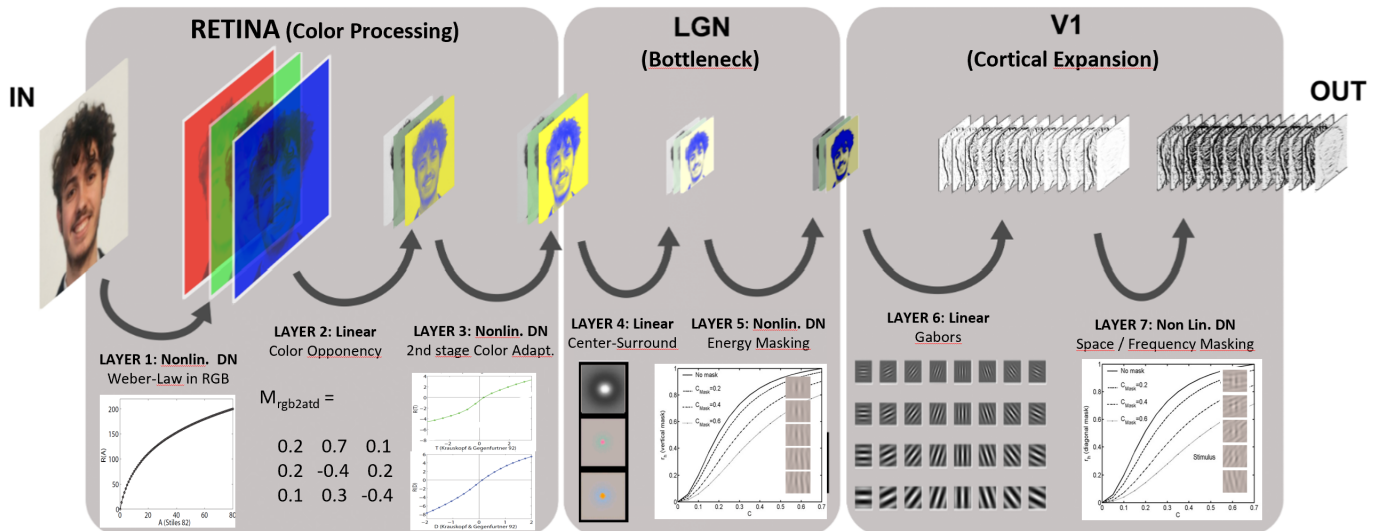


Fig. 1: **Scheme of the proposed *Parametric PerceptNet*.** The architecture is the same as in [63] but substituting each layer by its functional version. The figure illustrates the widely known stages of the retina-LGN-V1 pathway: inspired by visual neuroscience, it is a specific cascade of linear+DN layers as in [35], [37]. First, consistently with the Weber law, possibly happening in the LMS photoreceptors [70]–[72] the first (nonlinear) stage includes a DN [73], [74] in the input RGB channels. The second (linear) stage is meant to perform a transform to color opponent channels [75], [76], the third (nonlinear) stage is meant to implement the known adaptive nonlinearities of the RG-YB channels [77]–[80], the fourth (linear) stage applies center-surround kernels to the (eventually achromatic, red-green, yellow-blue) outputs of the previous stage because of what is known of the LGN [3], [4] and/or CSFs [1], [2], [5], [6]. The next (nonlinear) layer is a DN that is meant to represent generic energy masking of whatever frequency (i.e. in the spatial domain) [35], [41], [66]. The next (linear) layer applies Gabor wavelets because of the known shape of V1 receptive fields [9]–[14]. Finally, the last layer implements a final DN to accommodate the known spatial-frequency-orientation masking that happens among Gabor channels [24], [25], [31], [33], [34]. Note that at the V1 stages the linear gain of the Gabor filters (or scale of the final DN) is critical to keep the bandwidth of the system as described by the CSF [81]. Note also that the activation-like nonlinearities are all implemented using DNs as is natural in vision science [34]. These *non-standard* nonlinearities (unlike ReLUs or sigmoids) have parameters and are multidimensional [82]. This is represented by the fact that all nonlinear responses are not a single curve but multiple curves.

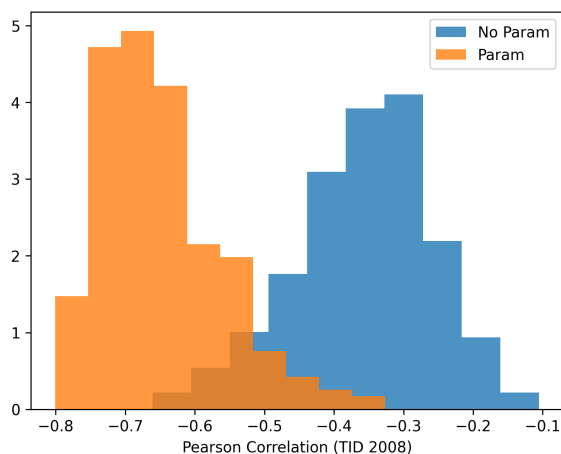


Fig. 2: **Positive bias induced by the parametrization.** Histogram of Pearson correlations between **100** random initializations of the parametric and the nonparametric *PerceptNets* and human opinion (TID2008). Larger negative correlation means more aligned with humans opinion.

version, *Parametric PerceptNet*. Fig. 2 shows histograms of the (Pearson correlation) performance obtained in TID2008. Throughout the work, correlations shown are negative because the distance measures obtained from the models try to reproduce the Mean Opinion Score **MOS** which corresponds to similarity, which is linearly related (with negative slope) with Difference Mean Opinion Score **DMOS**, which corresponds to distance.

By looking at the distributions we can see that the *Parametric PerceptNet* is better since it attains bigger correlations, and the distribution is sharper and peaks towards larger correlations. This result suggests advantages beyond the obvious reduction of parameters. First, the proposed parametrization includes a positive bias, which is not surprising given its inspiration in the referred vision science facts. Experiments below present explicit evidences that confirm this intuition. But also, as is known [92], parametrized deep neural networks allow to include physically meaningful restrictions in a very understandable and interpretable way. And this *problem-aware* approach is not as commonly seen in the conventional deep-net approximation to the image quality problem.

III. IMPLEMENTATION DETAILS

In this section we address five issues: (A) the conceptual and technical difference between training models with unconstrained tensors and models in which tensors have to follow a certain functional form. (B) The functional forms that appear in the biologically-inspired layers. (C) The issue of linear scaling of the linear and the nonlinear layers, which is important (as shown in the experiments below) both for the stability of the models during training and, more importantly, for their interpretability. (D) The specific 7-layer structure of the model, and (E) the psychophysically-meaningful values for their initialization.

A. Optimizing Parametric Models

Deviating from the traditional approach in deep learning of optimizing directly the weights of the tensors (or convolutional kernels) used during the calculations, in this work we propose to optimize a series of generative parameters that are going to be used to calculate the whole weight tensors.

By doing so, we can restrict our weight tensors to have a specific form of our liking, while reducing considerably the quantity of trainable parameters of our model. Even of greater interest is the fact that, by parametrizing the kernels of a convolutional neural network, we can independize the size of the convolutional kernels (both spatial and channel-wise) from the number of trainable parameters. This is impossible to accomplish within the traditional framework of optimizing each weight of the kernel.

Not only does this approach reduce the number of trainable parameters in our model. The most notable feature is that it allows us to introduce prior knowledge into the network in the form of the parametrizations chosen. This can be specially interesting when defining models that reproduce already known behaviors, as is the case when modelling the visual system. It is known that the Retina-LGN-V1 path can be modeled by a series of transformations that include applying center-surround and gabors filters, both of which can be introduced into a network as parametric convolutions. Moreover, more biologically plausible non-conventional activation functions can be employed. In our case we will use the divisive normalization [34], [93]. By imposing particular functional forms we remove the inherently "hopefullistic" approach employed normally when working with neural networks, based on which practitioners define certain architectures and train a model

hoping that its weights converge to a solution that can be considered good with regard to how similar it is to a certain known form. At the same time, parametrizing the kernels of the convolutional layers to desired forms allows us to impose a set of receptive fields that align well with human measurements and restrict the search space over which the network has to optimize its parameters.

This methodology introduces an extra step during training as the kernels have to be generated so that the gradient can reach the generative parameters. While it can incur in an increase of computational time, this cost can be reduced by parallelizing the generation of the kernels. When performing inference with the model, these kernels do not have to be calculated again, recovering the calculation speed of the non-parametrized models. A schematic representation of an optimization step within this framework is shown in Figure 3.

B. Parametric layers in deep nets based on Early Vision

In this section we describe the layers based on known functional forms that will be used by our model. We will define both the linear (based on convolutions) and the non-linear parts. For the linear parts we will define a functional form for the convolutional kernel, and for the nonlinear parts we will use a bio-inspired layer called divisive normalization (which can also include functional convolutions in its calculations) [34], [93].

Recent efforts to include parametrized biological computations into the models by construction are scarce [94]–[101]. And those approaches are very limited because they mainly rely on constraining, at most, partial aspects of the architecture and optimizing all the other model's parameters blindly [94]–[101].

1) *Convolutional Filters*: Usually a convolutional filter is defined as a tensor with $D_x \times D_y \times D_i \times D_z$ dimensions, where D_x and D_y are the spatial dimensions, and D_i and D_z are the input and output channels dimensions respectively. Instead of defining each position of the tensor as an isolated parameter (which is the conventional approach), here we are going to define parametrized functions that provide the values for each position of the tensor as a function of a reduced set of generative parameters.

We define a spatial function F in the spatial image dimensions (similar to pixel position) where we have two coordinates: $x \in R^{D_x}$ and $y \in R^{D_y}$. The specific shape of F is determined by some trainable parameters, Θ . Note that, opposite to the classical definition of the convolutional filter in neural networks, the number of parameters does not depend on the filter size.

For the input channels dimension we repeat the same spatial form, but we scale the values by a parameter $A_{iz} \geq 0$, i.e. $g(x, y, i, z, \Theta_z) = A_{iz}G(x, y, \Theta_z)$, similar to depthwise separable convolution. One could think on finding a different set of parameters Θ for each channel. However, we found our parametrization more convenient for different reasons: first, the number of parameters is smaller in our implementation. Second, it seems reasonable to combine features of the same spatial form of different channels. And third, this allows us to interpret the meaning of the learned filter more easily.

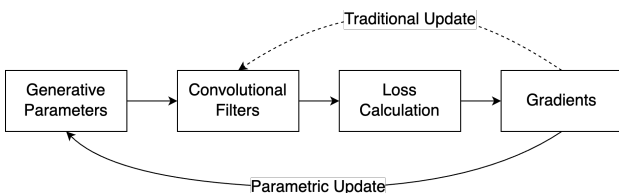


Fig. 3: **Illustration of an optimization step in a parametric layer.** The optimizable parameters are the generative parameters instead of the convolutional filters as a whole, which requires that we generate the convolutional filters at each step of the optimization so that the gradient can reach the generative parameters.

Each channel output of the convolutional linear layer will be:

$$X^{n+1}(x, y, z) = \mathcal{F}_{CL}(X^n, \Theta) = g(x, y, i, z, \Theta) * X^n(x, y, i) \quad (1)$$

Where X^n and X^{n+1} are the layer input and output respectively, and $*$ is the convolution operation in the spatial dimensions. Below we define the spatial functions chosen G , and how they are parametrized. As a general rule, the functional forms are centered with respect to the filter and normalized so that their energy equals 1.

a) *Gaussian Filter*.: A basic core function to the other functional forms that we use in this work is the classical Gaussian function:

$$G(x, y, \Theta) = e^{-\frac{1}{2} \left(\frac{(x-x_0)^2}{\sigma_x^2} + \frac{(y-y_0)^2}{\sigma_y^2} \right)} \quad (2)$$

This filter has two shape parameters, σ_x and σ_y , i.e. $\Theta = \{\sigma_x, \sigma_y\}$, and one scaling factor per input channel, $A_{iz} = \text{diag}(A_z)$. In practice, we optimize $\gamma = 1/\sigma$ for numerical stability.

b) *Difference of Gaussians (DoG) Filter*.: In Retina and Lateral Geniculate Nucleus (LGN) there are neurons that respond to center-surround (or difference of Gaussians) spatial shape [102]. It consists of two overlapped Gaussians with a shared center but with different sizes and signs:

$$G(x, y, \Theta) = \frac{1}{\sigma^2} \left[e^{-\frac{1}{2} \left(\frac{x^2+y^2}{\sigma^2} \right)} - \frac{e^{-\frac{1}{2} \left(\frac{x^2+y^2}{(K\sigma)^2} \right)}}{K^2} \right] \quad (3)$$

Center-surround mechanisms do not have orientation selectivity therefore, $\sigma_x = \sigma_y = \sigma$. Our definition (eq. 3) contains two parameters, σ and K , i.e. $\Theta = \{\sigma, K\}$. The scaling factors A_{iz} allows interaction between input channels but we chose to initialize them so that this interactions does not happen, i.e. $A_{iz} = \mathcal{I}$. In practice, we optimize $\gamma = 1/\sigma$ for numerical stability, and restrict K to be bigger than 1 during training to avoid changing the signs between the big and small Gaussians.

c) *Gabor Filter*.: Primary visual cortex (V1) simple cells transform information coming from LGN so that they are orientation selective [9], [10]. These cells have been modeled classically using a Gabor filter. A Gabor filter is a composition of a Gaussian filter multiplied by a sinusoidal grid:

$$G(x, y, \Theta) = e^{-\frac{1}{2} \left(\frac{\tilde{x}^2}{\sigma_x^2} + \frac{\tilde{y}^2}{\sigma_y^2} \right)} \cos(2\pi f(x\cos(\theta) + y\sin(\theta))) \quad (4)$$

Note that the gaussian is allowed to be oriented. In order to do so, coordinates are rotated as $[\tilde{x}, \tilde{y}] = R(\alpha)[x, y]$, where $R(\alpha)$ is a rotation matrix with angle α . This is equivalent to a symmetric covariance matrix. This way we have two parameters for the Gaussian shape, σ_x, σ_y , and one parameter for the Gaussian orientation, α . The sinusoidal grid has a frequency parameter, f , and an orientation parameter, θ . Note that we allow the gaussian and the sinusoid to have different orientations. In summary, the whole filter has five shape parameters, i.e. $\Theta = \{\sigma_x, \sigma_y, \alpha, f, \theta\}$. As in the *DoG*, the

scaling values A_{iz} are chosen so that there is no interaction between channels but could be optimized to do so. As in the other layers, we optimize $\gamma = 1/\sigma$ for numerical stability. This function allows different degrees of restriction in the parametrization which are discussed in Appendix A.

2) *Bio-Inspired activation function, Divisive Normalization*.: Activation functions are usually selected to be simple, fast to compute, dimension-wise and differentiable non-linear functions. While being differentiable and non-linear are mandatory features, being simple, fast to compute and dimension-wise are just convenient for implementation purposes. There are other non-linear activation functions much more aligned with biology. Our selected candidate is the divisive normalization proposed as a canonical operation in the brain [34]. Therefore, the output for each channel of the nonlinear layer in our model is defined as:

$$X^{n+1}(z) = \mathcal{F}_{NL}(X^n, \Theta_i) = B \frac{X^n}{(\beta + g(\Theta) * (X^n)^\alpha)^\varepsilon} \quad (5)$$

Where G is a convolutional filter that is applied to the input X^n in order to have an estimation of the magnitude of the neighbors. The parameter β is a bias parameter that avoids division by zero and controls how non-linear the operation is (among other things). The coefficient B allows the control of the output scaling. We fixed the values of the exponents, to be the same as in [91], $\alpha = 2$ and $\varepsilon = 0.5$. The parameters for each output channel in this layer will be the B, β , and the parameters of the filter G . In general G will be a Gaussian filter (eq. 2) which may depend on the parameters of the previous layer.

One advantage of using parametric functions is that we have direct access to the meaning of the outputs. For instance, we have direct access to the frequency, f , and the orientation θ of each Gabor filter. This can be used to design the following layer taking these parameters as input. This is what we do in the last layer of our model, where the divisive normalization kernel in the denominator depends not only on the spatial position but also on the other channels' frequencies and orientations. The denominator's idea is to have an estimation of the neighbors' magnitude, where these neighbors can be spatial, but can be also frequential, orientation, or chromatic neighbors. We use a simple Gaussian function where the distance in frequency and orientation is also taken into account (see eq. 6). As in the previous case, the different degrees of restriction allowed in the parametrization are discussed in Appendix A.

C. On the scaling of linear and nonlinear layers

Following Goodfellow's quotation mentioned in the introduction, control of the *linear scaling* of the linear and nonlinear stages is key in order to understand the *feature spreading problem* mentioned above. This will become apparent later in the discussion of the experiments.

In principle the linear scaling (or normalization) of *all* layers (both linear and nonlinear) should be explicitly controlled and be separately frozen or optimized if necessary. This is intuitively obvious in the linear cases: note that concatenation

of linear layers (or, if convolutional, linear filters) naturally introduces a competing uncertainty between the layers. The training may get trapped in a meaningless oscillation where one of the layers is amplified and the other is attenuated while not changing anything crucial (e.g. the shape of their frequency responses). The scale of the nonlinear layers has to be controlled in the same way for the same reasons, despite competition between scale parameters not being so interpretable between the nonlinear layers for obvious mathematical reasons.

In the *Parametric Perceptnet* we made particular choices to control this scaling, particularly in the layers that, in principle, seem more important from the texture point of view: the scale of the center-surround neurons, the Gabor neurons and the weights of the nonlinear DN after the Gabors. Imposing normalization constraints for the linear (convolutional) layers is trivial and it has also been proposed a general way for the DN transform [65]. However we did not systematically apply those constraints for consistency with the original nonparametric PerceptNet, where the scale of the DNs is not controlled in any way.

Regardless of the specific scaling choices made, detailed below, the experiments will show the critical implication of this kind of choices and how important they are to have explainable visual features in the models for image quality assessment.

D. The 7-layers structure of the Parametric PerceptNet

In this Section we describe the proposed Early Human Visual System (EHVS) model, which is fully parametric, i.e. each layer has a parametric function. Here we outline the function of each layer, while providing a more detailed explanation as well the number of parameters in each of them and their initialization values in Appendix B and C. Whenever padding is needed, symmetric padding is used instead of 0s because it improves the performance. We will follow the architecture of the model shown in Figure 1.

- **Layer 1 (DN - "Von-Kries / Weber adaptation")**: this layer mainly enhances low luminance ranges while compressing high luminance ranges following the idea in Weber law.
- **Layer 2 (Convolution - "Opponent Color Space")**: it is meant to reproduce the transformation to color opponent space. A spatial max pooling of 2×2 is applied after the transformation.
- **Layer 3 (DN - "Krauskopf-Genenfurtner Adaptation")**: This layer is inspired by the Von Kries color adaptation and is applied via a divisive normalization.
- **Layer 4 (Convolution - "LGN center-surround cells")**: applies a set of Center Surround receptive filters as seen in retina and the LGN []. This is implemented with a Difference of (Symmetric) Gaussians (DoG) (sec. III-B1b). A spatial max pooling of 2×2 is applied.
- **Layer 5 (DN - "Generic energy contrast masking")**: replicates the LGN normalization by applying a divisive normalization, where H is a parametric Gaussian kernel, independently to each input channel.

- **Layer 6 (Convolution - "Gabor receptive fields in V1")**: visual cortex (V1) simple cells modeled by applying the convolution operation between a set of parametric Gabor filters and the input. Each output channel corresponds to a specific frequency and orientation i.e. a different Gabor filter G . Mimicking the human visual system, we employ 64 filters for the achromatic channel and 32 for each of the chromatic channels.
- **Layer 7 (DN - "Space/frequency/Orientation masking in V1")**: divisive normalization in V1 that combines the outputs of the simple cells from the previous layer into complex cells. As the previous layer's filters are Gabors, we can define the denominator kernel so that there is a Gaussian relation between input features, taking into account not only the spatial position of the pixels but also the frequency and orientation of the features.

In total, the described model has a total of 1062 parameters.

IV. EXPERIMENTAL SETTING

In this paper we follow the classical approach for evaluating image quality metrics. We measure the correlation between the distortions predicted by the metric and the subjective distortions reported by human observers when rating the quality of a database of distorted images [41], [65], [103], [104]. We are going to consider 3 different databases: TID2008 [105], TID2013 [106], and KADID10K [107].

We follow the deep learning approach of training the models by maximizing the correlation with human ratings [44], [60], [91]. The 3 considered databases will be used as follows: TID2008 will be used for training our model, TID2013 will act as a validation set, and KADID10K will act as test set. We chose this configuration because TID2008 and TID2013 share the same reference images but have different distortions, so validating with TID2013 allows us to assess the distortion generalization capabilities of our model. On the other hand, KADID10K is chosen as test set because it has different reference and distorted images, so it can be considered as a good approximation to the image and distortion generalization capabilities of the model when deployed into the real world. Keep in mind that we will be using the smallest dataset to train our model, which is also interesting on its own because being able to obtain good generalization performances with as little training data as possible is always a thing to look out for.

Since these databases are collected among many observers and under loosely controlled observing conditions, each subjective rating has a lot of variance. In short, conventional databases are very useful but overfitting to them has no real point [65]. Therefore, it is important to have in mind the self consistency of the databases. Table I presents an estimation of the self consistency of these databases estimated with a simple Monte Carlo experiment. We sampled from a normal distribution with the mean and the variance of each subjective rating provided by the database¹. This simulates responses

¹The normal distribution assumption is just an option to do sampling. The actual distribution (which is not provided in the databases) may be non-Gaussian, and this would change the values a bit for the maximum attainable correlation, but the general conclusions would be qualitatively the same.

from different observers for the whole database, and we compute correlations (in particular Pearson ρ) between these "simulated observers". It is not reasonable that any metric should get a correlation bigger than the upper bound of these correlations (ρ_{\max}). Note that state-of-the-art metrics tuned to maximize the correlation usually obtain larger correlations than these estimated ρ_{\max} .

TABLE I: Size and self-consistency of some popular databases.

Dataset	# Samples	# Refs	# Dists	# Intensities	ρ_{\max}
TID2008	1700	25	17	4	0.86
TID2013	3000	25	24	5	0.83
KADID10K	10125	81	25	5	0.78

V. EXPERIMENTS AND RESULTS

In this section, we first analyze the effect of substitute each of the non-parametric layers by parametric bioplausible ones, and the effect of restricting the parameters values to be bioplausible or be fitted to maximize correlation. After that we analyze three versions of the model: one fully non-parametric, and two fully parametric one of them with the parameters restricted to be bioplausible and the other one fitting the parameters to maximize correlation.

We evaluate the three models in different terms. First we compare their performance with classical models following the classical approach (see Section IV). After we analyze their behavior during training. And finally, we interpret the three models in vision science terms by analyzing the performed transformations and the model features.

A. Relevance of each layer (ablation experiments)

In order to assess which of the modifications introduced produce better results, we perform an ablation study in which we parametrize different layers of the model and compare the results with an identical model without parametrization. We use the same kernel size for both the parametric and non-parametric model to keep the comparison as fair as possible. This results in a non-parametric model with many more trainable parameters and thus more learning capabilities, but we feel that using smaller kernel sizes would benefit the parametric model too much. To this effect we trained models with and without a parametrized center surround stage, with and without a parametrized divisive normalization after the center surround stage, with and without parametrizing the Gabors, and with and without parametrizing the last Divisive normalization. Note that we can only parameterize the V1 normalization (7) if we also parameterized V1 Gabor (6) because it needs to know the frequencies and orientations of its inputs and this information is only provided by the parametrized V1 Gabor layer.

Results in table II show that, in general, introducing parametric variations of different stages in the network does not hinder its performance. All models perform above the human-like correlation of Table I. Interestingly, all the models that perform better than the Non Parametric version include the parametrized V1 Gabor layer (6). This shows that enforcing Gabor receptive fields at this stage of the network is a

reasonable bias and improves performance. As opposed to this, including the parametrized DoG layer (4) results in a decrease in performance. This may point to an interaction between the DoG and V1 Gabor layers (a special case of the *feature-spreading problem*) that should be given special attention in further work.

This is not surprising because while center-surround receptive fields represent circularly symmetric filters that may be band-pass or low-pass in the Fourier domain, combinations of Gabor filters (as shown in the simulations below) include those possibilities and many others. This implies that Gabor filters alone *may do the role of (or substitute)* center-surround receptive fields. Not the other way around: that is why including Gabors is more important than including the center-surround cells. This redundancy that is certainly present in the visual system [3], [4], [9], [10] has a negative effect (when the systems are trained *just for correlation with the MOS concept*). This is particularly interesting because the existence of center-surround cells in the LGN (the bottleneck of the retina-cortex pathway) may be due to *other reasons*: a number of authors have argued that these cells (or the equivalent CSFs) are there to enhance the retinal signal [5], [6], [108], [109]. And setting the global frequency bandwidth (as done by the LGN) may be necessary before the Gabors that come in V1 (after the bottleneck) start to analyze the shapes by breaking the Fourier domain into pieces.

Contrary to common expectations, the model with more parameters is not the model that performs better either at training or validation. One may attribute this to the fact that, even if the Non Parametric model can converge to the parametrized solution, having so many parameters makes this very hard from an optimization perspective. Finally, we see that including the B coefficients (layer 8) to the fully parametrized model results in a performance increase. This would not be the case in a Non Parametric model because the same output could be obtained by scaling the learned weights, but becomes helpful in the parametric scenario because the scale of the weights is bound to the functional forms used to generate them. With the evaluated parameterizations we are able to obtain models with only 5k parameters that perform better than a model with more than 7.5M. The most notable reduction in parameters comes from parametrizing the V1 Gabor [6] and V1 normalization [7] layers.

B. Distance to optimum (selective freezing experiments)

In this experiment, we try to assess "how far" is our handcrafted initialization from a good set of parameters that result in human-like performance. It is important to remind the reader that producing an interpretable handcrafted initialization is only possible because the model has a reduced set of easily interpretable parameters. It would be considerably harder to initialize the weights of a 7-layer convolutional model by hand in an interpretable way. To do so, we will initialize the model and train different versions of it where we only let the optimization algorithm change the parameters from a particular layer onwards. The initializations are chosen assuming that the previous layers behave in a particular way,

TABLE II: Ablation analysis changing parametric layers for their non-parametric counterpart, pearson correlation is shown. The numbers in brackets indicate which layers are parametrized. Models that perform better than the Non Parametric version are highlighted in bold.

Param. Layers	TID2008	TID2013	# Params
Non Parametric	-0.961	-0.899	7598852
[1]	-0.952	-0.893	7598848
[1, 4]	-0.939	-0.897	7594910
[1, 5]	-0.935	-0.903	7598495
[1, 6]	-0.965	-0.906	7230280
[1, 8]	-0.955	-0.895	7598976
[1, 4, 5]	-0.949	-0.901	7594549
[1, 4, 6]	-0.944	-0.892	7226342
[1, 4, 8]	-0.946	-0.908	7595038
[1, 5, 6]	-0.942	-0.902	7229927
[1, 5, 8]	-0.940	-0.897	7598623
[1, 6, 7]	-0.963	-0.906	5233
[1, 6, 8]	-0.945	-0.901	7230412
[1, 4, 5, 8]	-0.944	-0.901	7594677
[1, 4, 6, 8]	-0.947	-0.893	7226470
[1, 4, 5, 6]	-0.929	-0.891	7225985
[1, 4, 6, 7]	-0.926	-0.891	1295
[1, 5, 6, 7]	-0.958	-0.903	4880
[1, 5, 6, 8]	-0.970	-0.902	7230055
[1, 6, 7, 8]	-0.957	-0.906	5365
[1, 4, 5, 6, 7]	-0.926	-0.887	938
[1, 4, 5, 6, 8]	-0.935	-0.891	7226113
[1, 4, 6, 7, 8]	-0.930	-0.896	1423
[1, 5, 6, 7, 8]	-0.975	-0.898	5008
[1, 4, 5, 6, 7, 8]	-0.928	-0.890	1062

so we won't be trying different combinations as in the previous experiment.

Results in table III show what it is to be expected: the more freedom we give the algorithm to change the parameters, the better performance we get. On the other hand, this comes at the cost of obtaining not so understandable parameters. The most important take-away is that even in the most restricted scenario (i.e. all the parameters set by hand but the B coefficients in the last layer), we are very close to the previously calculated human-like performance. This supports the idea that human-like performance can be attained when constraining the parameters to be human-like but may differ considerably when pushing the model's performance into super-human territory.

C. Models selected for further analysis

Given the good results in correlation obtained by all the models, we select three configurations to be further analyzed in the following section. We make such selection because it represents the path between two extremes: on the one hand, the current conventional unconstrained approach, and on the other hand, the classical frozen extreme where all parameters are taken from a range of disconnected experiments of the visual neuroscience literature and put together without further optimization. Namely,

- **Non-Parametric Perceptnet (Non-Param)**. All the layers are non-parametric, similar to the original PerceptNet. The only thing that changes is the size of the convolutional filters to match the size of the parametric ones.
- **Parametric bio-initialized and fully trained (Param-Fully)**. Parametric model where the parameters

of all layers have been initialized to be biologically plausible (using values in Table V) but after that, *all* parameters are fitted to maximize the correlation with MOS in TID2008.

- **Parametric bio-initialized but just last scaling trained (Param-Partial)**. Parametric model where (as above) the parameters of all the layers have been chosen by hand, but then only the simple linear scaling of the last layer (the B coefficients in Eq. XX) is optimized for correlation with MOS. In this way we ensure that the model reasonably behaves according to the classical literature on human vision. Note that leaving a final linear scaling stage to be optimized after the application of Gabor filters also is psychophysically sensible. For example, such final stage after Gabors has been optimized to reproduce the Contrast Sensitivity Functions [110].

D. Behavior in training: stability and overfitting

The experiments here show that the parametric models train faster, smoother, and show better regularization than the non-parametric version. Arguably, this can be attributed to the fact that they are better initialized and their optimization landscapes are more restricted.

Figure 4 shows the learning curves for the three analyzed models (Sec.V-E). As expected, parametric models start from a better position, converge faster with softer curves, and show the regularization effect of the parametrization. This can be attributed to the fact that the parametrized models have many less parameters which are initialized closer to the solution. At the same time, the parametrization acts as a regularization potentially smoothing the optimization landscape. This validates the chosen parametric forms.

The non-parametric model takes much longer to converge and overfits, which is easily visible in Table IV, where it obtains much bigger correlation than the maximum experimental one in train and validation, but the performance is reduced in test. The parametric fully trained model gets similar results as the non-parametric while having 3 orders of magnitude less parameters. However, in Sec. ?? we will see that it converges to a set of parameters that are not as human-like as one could expect. As the bio-fitted model trains only the coefficients of the last layer to adjust the importance of each channel (128 params), it obtains lower performances but suffers less from overfitting while performing as the non-parametric model in test. The training process is smoother and faster than the other models, and the results are fully interpretable as we will see in Sec. V-E.

E. Experiments for feature visualization and interpretability

In this subsection we present two results with the selected models mentioned above after biologically inspired initialization and optimization to maximize the correlation with human ratings: First, (1) we take an illustrative natural image (with opponent colors, textures and a synthetic shadow to induce a spatial variation of contrast). We visualize the responses to this specific stimulus in order to discuss (in the next section) if the responses qualitatively capture the known facts of the low-level

TABLE III: Performance of the model when freezing the initialization up to different depths in the architecture. The numbers in brackets indicate the frozen layers. It is clear to see that the more restrained the model, the lower performance it attains. What is to be taken into consideration is that even the more restricted model is achieving what we obtained as the human performance in I. This hints that the initialization we proposed is close to a good solution.

name	TID2008	TID2013	KADID10K	# Params.	# Trainable Params.
Fully Trained	-0.926	-0.882	-0.797	1062	1062
[1]	-0.922	-0.877	-0.767	1062	1060
[1 - 2]	-0.910	-0.881	-0.789	1062	1051
[1 - 3]	-0.886	-0.864	-0.776	1062	1045
[1 - 4]	-0.886	-0.855	-0.745	1062	1018
[1 - 5]	-0.863	-0.835	-0.729	1062	1009
[1 - 6]	-0.847	-0.818	-0.708	1062	553
[1 - 7]	-0.829	-0.808	-0.713	1062	128
[1 - 8]	-0.417	-0.463	-0.527	1062	0

TABLE IV: Performance of the final models chosen together with some state-of-the-art perceptual quality metrics. (*) indicates that the models were trained in that particular dataset.

Model	TID2008 (Train)	TID2013 (Validation)	KADID10K (Test)	# parameters	# trainable parameters
Non-Parametric	-0.961*	-0.899	-0.755	7,598,852	7,598,852
Param. Fully Trained	-0.928*	-0.890	-0.796	1062	1062
Param. Bio-Fitted	-0.829*	-0.808	-0.713	1062	128
SSIM	-0.653	-0.724	-0.660	3	3
LIPS	-0.697	-0.732	-0.700	14,714,688	1472
DISTS	-0.803	-0.832	-0.857*	14,714,688	2950
Max. Exp. Corr.	-0.86	-0.83	-0.78		

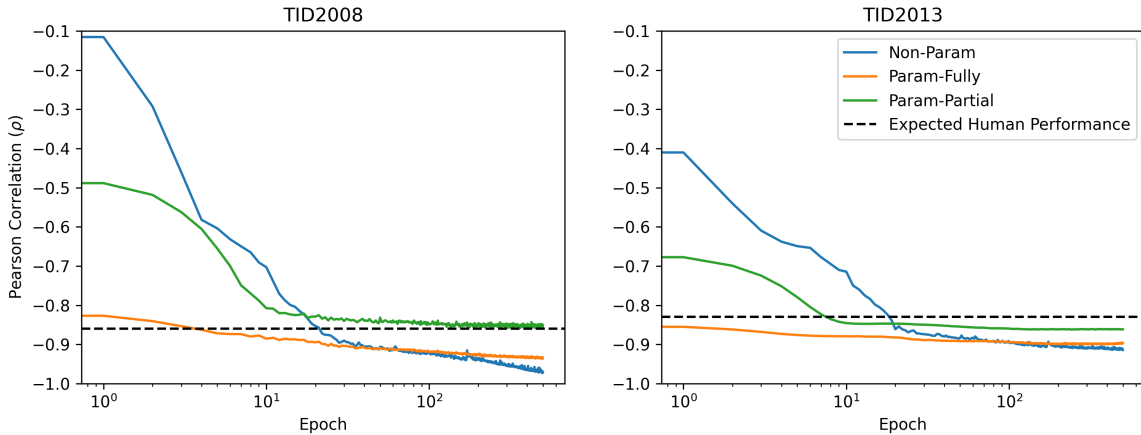


Fig. 4: Learning curves for the three selected models. Training is performed in TID2008 while TID2013 is used for validation. Results in test can be seen in Table IV

psychophysics known to happen in the retina-V1 pathway (that we are arguably supposed to be modeling). Then, (2) we go through all the layers after optimization and we visualize their kernels (receptive fields), nonlinear responses, and optimal features found. The biological plausibility of such results will be discussed in the next section.

1) Responses to an illustrative natural-synthetic image:

We'll start by describing the input image shown at the top of Figure 5. This image has been chosen to illustrate a range of known psychophysical phenomena. First, the natural part of the image (the standard Parrots image [111]) was chosen because it has objects whose colors (basically) are in the known opponent red-green and yellow-blue directions [8], [76] and can be used to check if there are layers tuned to these relevant visual facts. Then, the periodic patterns were chosen

to have 4 and 8 cpd respectively ², and they are oriented at 0 and 45 degrees. These textures (known to induce optimal stimulation in certain regions of the V1 brain [11], [33], [112]) were chosen to check if the responses of the different layers are specifically tuned to these kind of patterns. Then, a controlled shadow has been added to the picture. This shadow is generated through controlled variations of the luminance and the contrast of the chromatic channels across the image. First we reduced the luminance in the left part of the image in order to check the the known Weber-law, which enhances the response in the low luminance regions and moderates the response in the high luminance regions [70], [72], [113]. Finally, the contrast of the left part has also been reduced to check if the models fulfill the (known) fact that visual

²In this example the sampling frequency has been chosen assuming that the image is observed at a distance so that it subtends 4 degrees of visual angle.

system increases its sensitivity (or boosts the responses) in the low-contrast regions [33]–[35], [65]. While the luminance has been changed by taking into account the tristimulus-to-digital-values correction and simply reducing the mean in the achromatic channel of a psychophysically-meaningful opponent color space [8] (keeping the mean of the chromatic channels the same), the modification of the contrast is more delicate. This is because contrast and colorfulness perception is not independent of the luminance [72], [114]. Therefore, contrast has been modified by using an RMSE definition of contrast based on the ratio between the standard deviation and the mean of an image which is applicable to natural images and reduces to the classical Michelson contrast for sinusoids [115]. This modification was not only made in the achromatic channel (as mentioned above for the luminance), but also applied in the chromatic opponent channels not to introduce non-natural variations of colorfulness in the image. The Matlab code to generate this image is available here³.

The different rows of Figure 5 after the input image (from top to bottom) show the response to the input as it is represented in each layer of the models. The panel in each macro-column represents the results for each model: *Non-Param*, *Param-Fully*, and *Param-Partial*. Figure 6 shows a zoom of the responses for the first 16 sets of neurons of the models (those that in the parametric models were initialized to be tuned to achromatic features and four frequencies and four orientations according to the prescriptions of classical models [14], [35], [118], [119]). Figures 7 and 8 show the *input-output* response curves and the *parametric receptive fields* of the corresponding layers. The input-output response curves are represented using scatter plots of the signals shown in Figs. 5 and 6.

The model that best reproduces the saturating non-linearity (corresponding to Weber law) is the Param-Partial model. It can be observed that the dark parts of the image have been lightened by increasing the brightness of regions of low input luminance, while the bright parts of the image are not amplified and the relative proportion of the responses and the equivalent colors have not been modified. The relationship between the red, green, and blue primaries has not been modified in this model. However, in the Param-Fully model, as will be seen later, the input-output response curves are basically linear, and although there is a certain luminance equalization, this equalization is less pronounced than in the Param-Partial model.

To finish with this first row, on the left (non-parametric model), there are no biologically significant characteristics. On one hand, the relationship between the scales among the primaries has become unbalanced. And, on the other hand, because the response is basically linear, the image brightness has not been modified in the stage that should correspond to the linear transformation of color opponency. It can be seen that the Param-Partial model effectively executes this computation. This is not surprising, given that the opponent matrix is applied to the red, green, blue primaries, so that the left image corresponds to luminosity. The central image

corresponds to the red-green channel, as can be seen in the parrot, and the right image corresponds to the blue-yellow channel, so that the blue part of the wing is dark due to the blue component, and the reddish part of the chest and the parrot’s head appears with high amplitude due to the yellow component of that area of the image region. In other words, the opponent transformation is perfectly implemented. However, in the Param-Fully model, the receptive fields of the opponent transformation have been deformed in such a way that their meaning is not biologically plausible. This is also observed in the non-parametric model.

In the adaptation stage that should represent the non-linearities reported by Krauskopf and Gegenfurtner, in the Param-Partial model, we see that the images are not modified due to initialization through a basically linear transformation. This is also the case for Param-Fully model.

It seems that these non-linear stages are not relevant to achieving the chosen objective in this case, that is, maximizing the correlation of human opinions in subjectively evaluated databases, and therefore the optimization does not modify the linear initialization in these cited cases nor in the non-parametric case.

The next stage consists of the application of center-surround receptive field neurons. In the Param-Partial model we can clearly see the difference in neuron behavior: low-pass in the chromatic channels due to the strong blurring of the red-green and blue-yellow channels. Meanwhile, we can observe the band-pass behavior in the image corresponding to luminosity. Notice how edge enhancement has occurred in the natural image area, and also note that low-frequency patterns have been preserved, while the contrast of high-frequency patterns has been reduced. These patterns have totally disappeared in the red-green and blue-yellow images due to the low cut-off frequency of the sensitivity functions. At the same time, we can observe that the cut-off frequency of the achromatic contrast sensitivity function is much higher than the chromatic ones.

On the other hand, in the Param-Fully model, although the initialization has been the same as in the Param-Partial case, the frequency behavior of the center-surround neurons has diverged from the biologically plausible initialization, as observed in the fact that all periodic patterns have been attenuated more or less with the same intensity. Finally, the non-parametric model also reflects this arbitrary distribution of bandwidths among the three channels which has no defined chromatic meaning.

Finally, the non-linear stage that has been implemented after the center-surround neurons has a contrast enhancement behavior in regions whose input has low contrast. For example, in the left region of the image where the parrot was not clearly discriminated in the responses of the previous layers, especially in the achromatic channel.

In this case, the parrot’s head starts to become visible, and this effect is observed much more clearly in the increase of responses corresponding to the inputs of periodic patterns that have low contrast in the left part of the image. This biologically plausible behavior, consistent with multiple references in the biological literature, is not observed with the same intensity

³loretes.m which uses the Matlab toolboxes Colorlab [116] and Vista-lab [117].

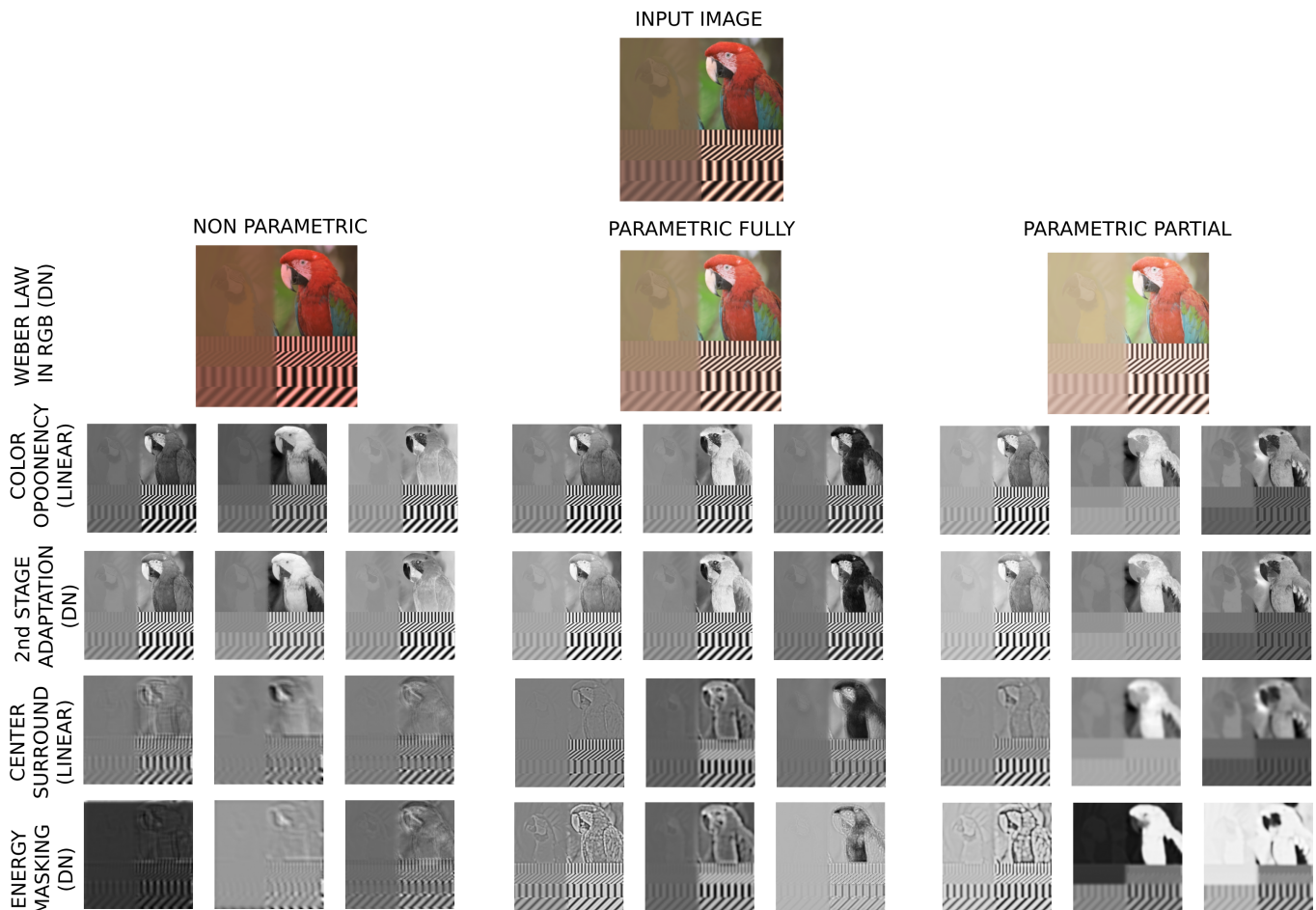


Fig. 5: **Input image represented in each layer of the model (Retina-LGN).** Each column represents the results for each model: *Non-Param*, *Param-Fully*, and *Param-Partial*.

in the Param-Fully model nor, of course, in the non-parametric model.

2) *Visualization of features and nonlinearities:* In Figure 6 we see the set of analyzers that should model the primary visual cortex, both before divisive normalization in the upper panels and after divisive normalization in the lower panels, corresponding to the application of linear filters, followed by the non-linear computation of divisive normalization.

In the case of the Param-Partial model on the right, the responses highlighted by blue and green squares show two interesting things in the first upper panel. It is observed that different outputs from the Gabor layer correspond to characteristics tuned to different frequencies and orientations. For example, the square in green shows a strong response to vertical-type patterns of different frequencies. Similarly, the square in blue shows that each of these filters responds to patterns of the same frequency but different orientation. On the other hand, in the lower panel, we see the response corresponding to the output of these neurons after the divisive normalization interaction that locally mixes different spatial positions and different characteristics.

The effect described, for example, in [34], [65], states that the effect of divisive normalization consists of enhancing the

response in regions where the input has small amplitudes corresponding to small contrasts, something that is seen in how the oscillations of the responses increase.

How does the amplitude of the responses increase in the left region of the input image that corresponds to a zone of low contrasts? This behavior, which is biologically plausible and observed in the Param-Partial model, is not observed at all in the Param-Fully model despite having the same optimization objective. For example, although the regions marked in red and orange do respond to specific frequency patterns, as seen in the upper panel, it is observed that after divisive normalization, the scale of the responses don't make much sense: the band highlighted in red has completely disappeared, while in the band highlighted in orange, although a small increase in the amplitude of the responses is observed in the left region of the image, this contrast enhancement in the responses is not as intense as in the parametric case, as can also be seen in the subband highlighted in yellow. Finally, since in the non-parametric model the linear filters have no particular physical meaning, the responses have no qualitative sense, as seen in the illustrative examples highlighted in pink in the upper panel.

Likewise, divisive normalization basically has no effect, as seen in the equivalent subbands highlighted in pink in

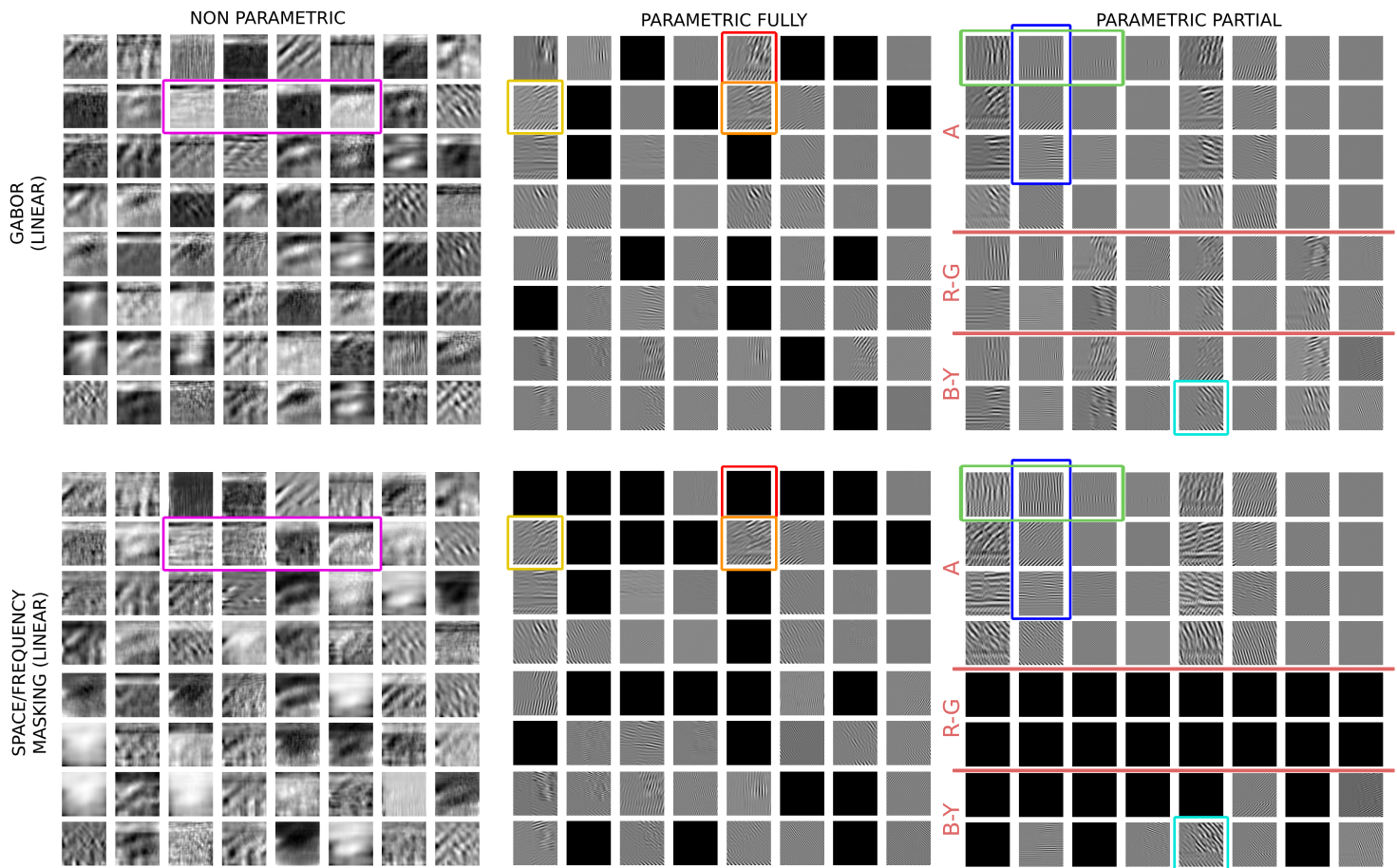


Fig. 6: Image represented in the last layers (linear-V1 and nonlinear-V1): after the conv 3 (Gabor) and DN4 (V1 Normalization). Only the first 16 of 128 outputs are represented for proper visualization. Each of the three columns represents the results for each of the three models: non-parametric, parametric bio-fitted, and parametric psychophysically fitted. While the results. In the case of the non-parametric model the outputs does not resemble to the outputs of orientation and frequency selective filters, while in the parametric ones this is imposed (and achieved). The bio-fitted model has a clear multiscale and multiorientation representation, while the parametric trained one is more diffused and actually some outputs are discarded by the model at this stage.

the lower panel. The input and output responses observed in Figure 7, as well as the receptive fields, are consistent with the type of responses visually represented in Figures 5 and 6. Specifically in the stage that should represent Weber’s law of saturation.

The Param-Partial model presents the more saturated input-output curves. Likewise, we see that saturation is disappearing in the Param-Fully model, indicating that this non-linearity is not relevant to solve the training set used, although it would obviously be relevant in general, especially in high dynamic range images. Finally, in the non-parametric model, the non-linearity has almost completely disappeared and, furthermore, the scaling between the different red, green and blue channels does not respect the relative scaling, producing a modification of the chromatic information in the scene.

In the basis change matrix from RGB space to what should be opponent channels, it is seen that only in the Param-Partial model the biologically plausible transformation is respected for obvious reasons, because it has been imposed. However, the error made in the Param-Fully model in the achromatic channel is striking, where what would be equivalent to the trichromatic units in the first row of the transformation matrix (if

this first row corresponded to an achromatic sensor) is giving much more relevance to the red channel that really doesn’t have as much weight as the green and blue channels, and this is biologically incorrect. On the other hand, we see that the central channel is basically a red minus green minus blue channel, when in reality it should be red minus green. The last one is green, blue minus red, which also doesn’t correspond to the blue-yellow channel. Finally, in the non-parametric model, although there is a basically correct first achromatic channel, the other channels are random.

The second stage of adaptation doesn’t have a clear interpretation, and the analysis of the receptive fields of the three models is much more interesting in the case of the Param-Fully model. We can observe the center-surround function in the achromatic channel and we can observe Gaussians of larger amplitude and, therefore, lower cutoff frequency in the red-green and blue-yellow channels. Following, we see spatial Gaussians in the divisive normalization responsible for reproducing the masking effect. In the case of the Param-Fully model, despite an understandable initialization, it is seen that it diverges to a solution that is difficult to interpret, in no case with biological significance. Finally, in the non-parametric

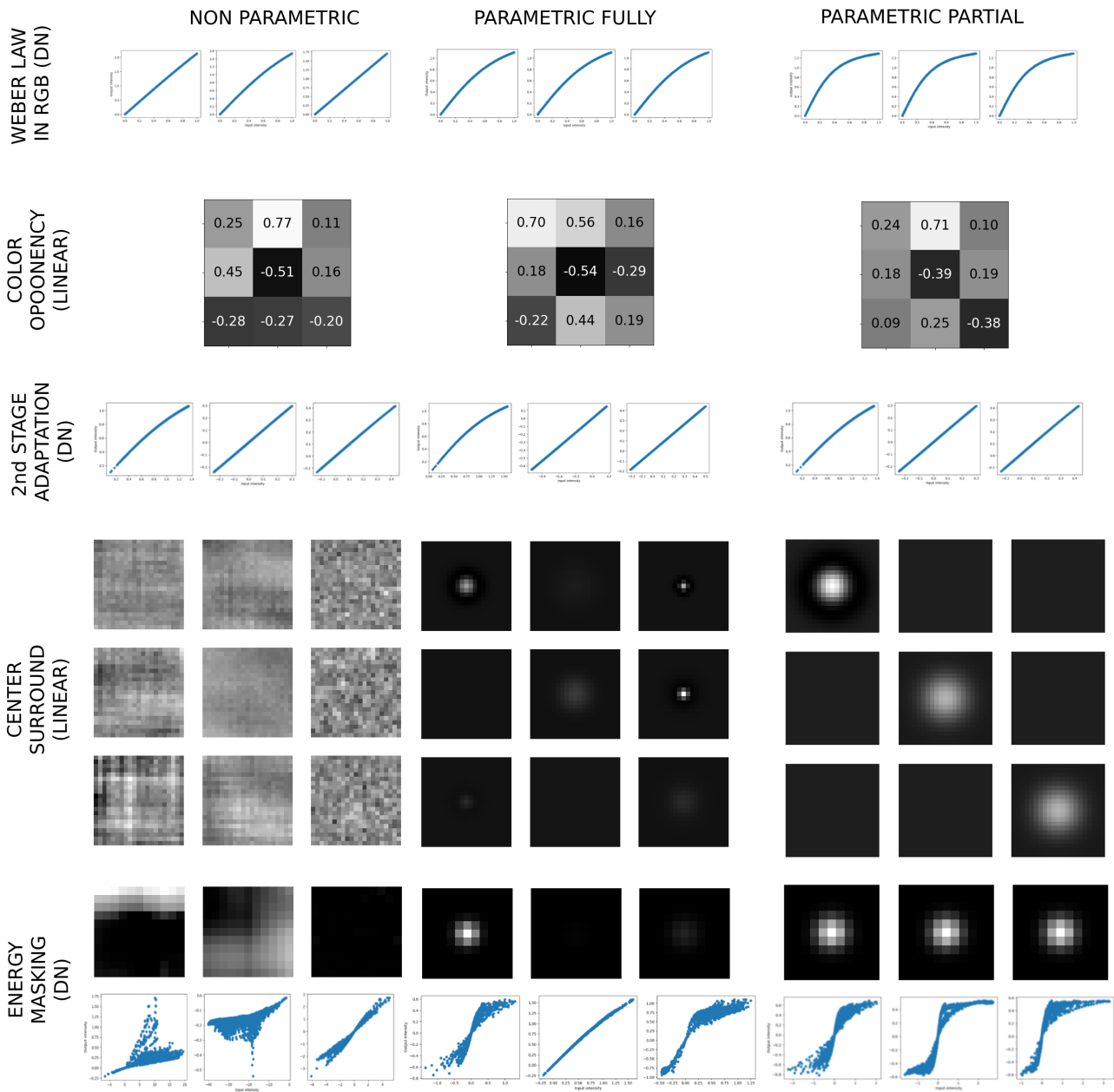


Fig. 7: **Input-Output Response Curves and Parameters (or receptive fields) for the Retina-LGN layers.** In each row we can see the effect of the layer over data. In the non-linear stage a input-ouput function over a natural image (the one from figure 5) is shown. For the linear stage the convolutional filters are shown. Each of the three columns represents the results for each of the three models: non-parametric, parametric bio-fitted, and parametric psychophysically fitted. The transformations performed by the bio-fitted model are consistent with the literature. However it is not the case for the other two.

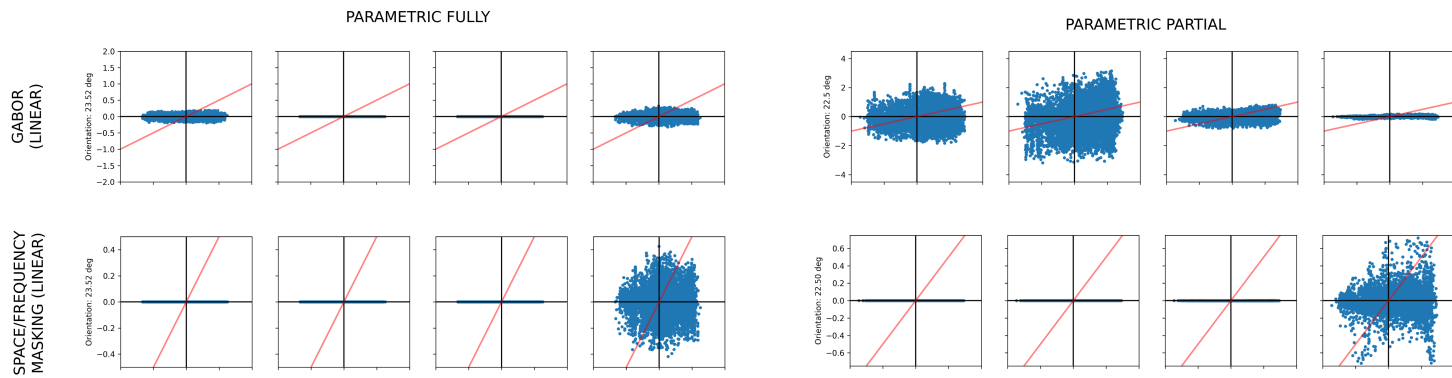


Fig. 8: Input-output Response Curves for the linear-V1 and nonlinear-V1 layers. In this case we only show a subset of all possible input-output responses for the Gabors of 2, 4, 8 and 16 cpd (for a fixed orientation). As in the case of the non-parametric PerceptNet this identification is not possible, only the input-output responses of fully trained and the partially trained parametric PerceptNets are shown (before -top- and after -bottom- scaled Div. Norm.).

case, nothing in particular can be remarked since it has no defined structure.

It can be seen that, in the Param-Partial model, there is a saturating and adaptive behavior with respect to the positive and negative values of the input, which has a very adequate biological interpretation. The non-parametric case, effectively, makes no sense. And, in the Param-Fully model, it is curious that in the first and third channels, there is more or less saturation, as in the biologically acceptable case. However, the central channel of the second has a more linear behavior, something that makes no biological sense.

Finally, in Figure 8, we observe the input-output curves of the different Gabor filters before the application of divisive normalization in the upper panels and after the application of scaled divisive normalization in the lower panels.

Note that the only behavior that makes biologically plausible sense is that of the Param-Partial model because, taking into account that the x-axis in all cases has the same amplitude, the distribution of samples on the x-axis has the same amplitude regardless of spatial frequency because in that axis the input corresponds to the amplitude of the image in the spatial domain. However, on the y-axis we have the response of filters of different frequencies and it is observed that, in the upper right panel, filters sensitive to relatively low frequencies amplify the signal in a moderate way. While those of medium frequencies (four cycles per degree) are the ones that amplify the signal the most. This is consistent with the fact that the maximum of the contrast sensitivity function is found around a frequency of four cycles per degree. When we consider higher frequencies such as eight cycles per degree (third graph) or sixteen cycles per degree (fourth graph), the amplitude of the responses progressively falls, clearly indicating the bandpass character of the contrast sensitivity function of the achromatic channel.

This behavior is not visible in the Param-Fully model shown in the upper left panel. It is very interesting that, after the application of scaled divisive normalization, both models reach a totally equivalent gain in these different channels, indicating that this particular configuration is optimal for maximizing

correlation with human opinion in the databases used. Despite the fact that this particular distribution of responses makes no biological sense, Figure 9 represents the parameters of the linear and non-linear layer corresponding to the part of the model that should represent the primary visual cortex.

This figure has two panels: first, on the left we see each of the receptive fields and, in the center, the dark squares represent the sum of the Fourier transforms of the receptive fields. In parametric cases, the first 64 elements correspond to the achromatic channel, the next 32 to the red-green channel, and the last 32 to the blue-yellow channel. The figure located below corresponds to the Gabor-like filters weighted by the amplitude of the transformation of the divisive normalization of the last cortical layer.

Analyzing this figure we can see that while in the Param-Partial model, the receptive fields are perfectly organized and make good biological sense, that is, there is no interaction between the different achromatic and chromatic channels, in the Param-Fully model, it is observed that the weights of each of the channels have changed so that this is no longer maintained and, therefore, the biological sense has been lost.

This is evident in the sum of the Fourier transforms of these receptive fields. In the Param-Partial model, we have contrast sensitivity functions, that is, the sum of the Fourier transforms of the preceptive fields approximately reproduce the achromatic contrast sensitivity functions before being weighted by the final weights that have been optimized. It is noteworthy that the weighting of these optimized weights destroys the behavior that was biologically reasonable. In the Param-Fully model, the sum of the Fourier transforms of the receptive fields makes no sense either before divisive normalization or after, needless to say in the case of the non-parametric model the results have no biological meaning. This consistency with biology or inconsistency can also be observed in Figure 10 although, in this case, the interpretation is more confusing due to the saturation that corresponds to the limits of digital images. Regarding the optimization of response maximization, therefore, this conventional visualization figure will not be analyzed here in greater depth.

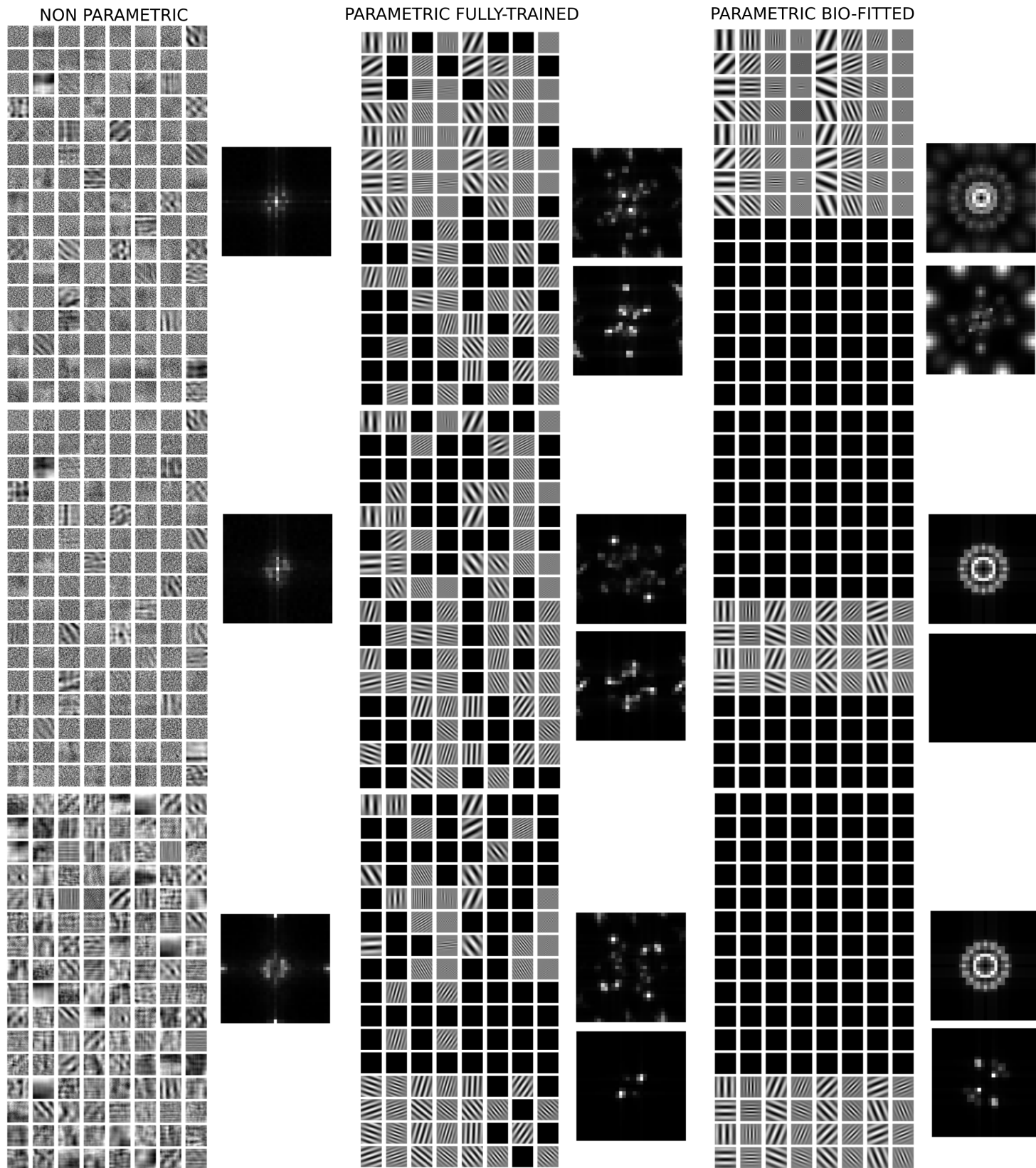


Fig. 9: **Models Parameters (or receptive fields) for the last Gabor-like layer.** Each of the three columns represents the results for each of the three models: non-parametric, parametric bio-fitted, and parametric psychophysically fitted. Each row shows the filters for each of the input channels. In the bio-fitted model the filters act independently to each input channel. The Fourier transform of all the filters combined are given for each model and channel.

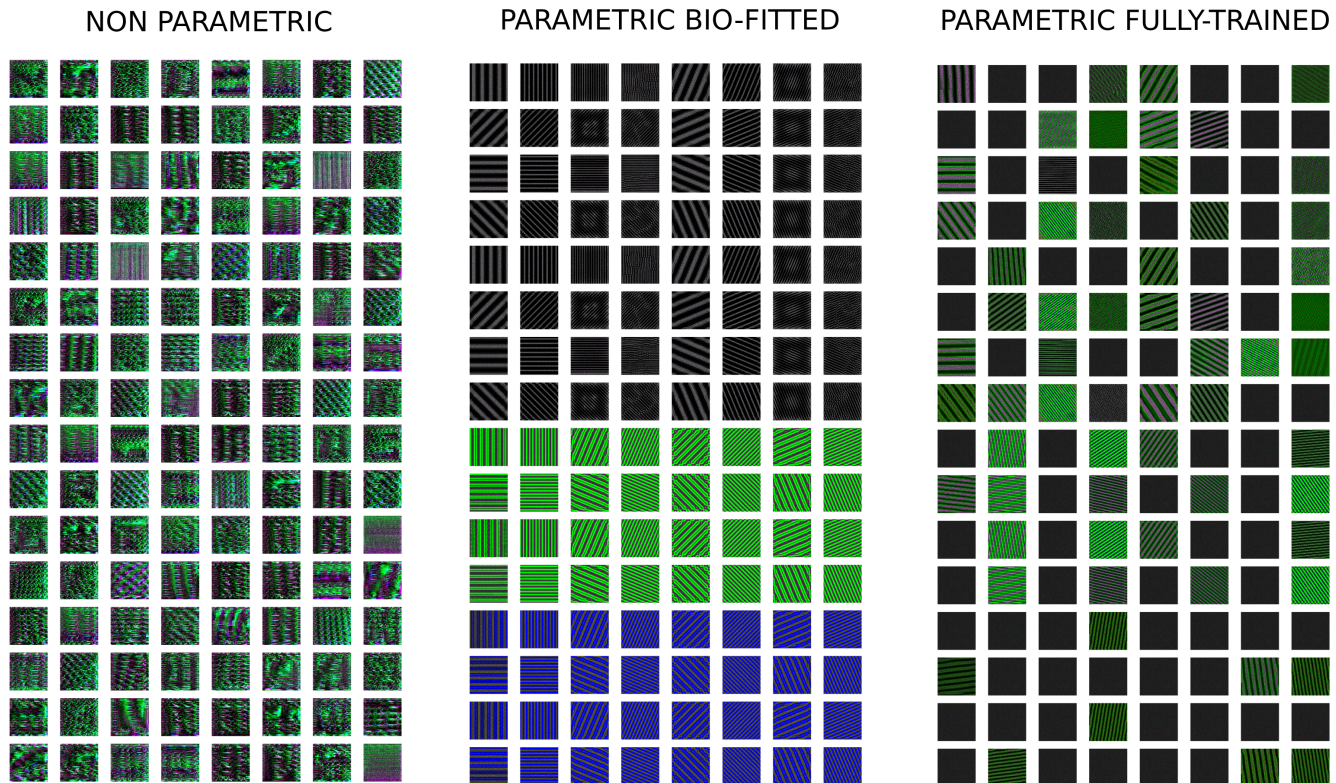


Fig. 10: **Conventional visualization of features of the Gabor-like layers.** Specifically, an image that makes maximizes the response of each of the 128 outputs is shown. Each of the three columns represents the results for each of the three models: non-parametric, parametric bio-fitted, and parametric psychophysically fitted. In the bio-fitted model the filters clearly correspond to a frequency and orientation selectivity filters, with different chromatic sintonization, 64 achromatic filters and 64 chromatic ones (32 red-green and 32 blue-yellow). For the other models the filters are biased to the red-green in both cases which can be the case for the training dataset TID 2008.

The destruction of the biological plausibility of the receptive fields, on one hand, and of the scaling introduced on the dynamic range of divisive normalization, can be seen in Figure 11. Here we see that the biologically plausible distribution shown in the upper section, where we see the distribution in octaves of the frequency sensitivity of different channels, both in the achromatic channel in the upper part and in the chromatic channels in the lower part, and the orientation sensitivity are completely destroyed after optimization in the lower panel, and a series of random values appear that have no biological meaning when proceeding to optimize the scales of the dynamic range of divisive normalization.

VI. DISCUSSION

The results of the experiments we just showed illustrate two important things. The first is obvious: if you input the parameters indicated by classical perception literature into the model, you obviously obtain biologically plausible behavioral results from the model and also good performance in predicting human distortion measurements in subjectively evaluated databases.

However, on the other hand, if we adjust overly flexible models, we get a quantitatively similar result for this objective but, when analyzed in detail, the behavior is not human at all and, therefore, we see two conclusions.

One is that the proposed objective is not demanding enough to constrain the models in a way that reproduces the known behavior of visual pathways and, on the other hand, it illustrates something much more interesting that the deep learning literature has not analyzed in depth: the feature spreading problem. This is qualitatively introduced in the first part of the work and illustrated here in the experiments we just saw. Despite being a parametric model with an extremely reduced number of parameters and having a biologically meaningful initialization, the redundant nature of the proposed model makes the characteristics to which the system must be sensitive to solve the problem spread uncontrollably throughout all layers of the network, resulting in a model that is difficult to understand qualitatively and lacks biological meaning. This is the most important conclusion of the work in this discussion.

Apart from indicating this fact we present two interesting final results, the first of which is shown in Figure 12. This figure explains the limitations observed in the response of some layers, particularly the layer corresponding to the non-linear processes that eventually occur in the retina, and the layer corresponding to the non-linear processes that should appear after the opponent chromatic transformation. As we've seen in the results, these layers don't have a completely satisfactory biological behavior, but this can be exclusively attributed to the fact that, to make a fair comparison with the

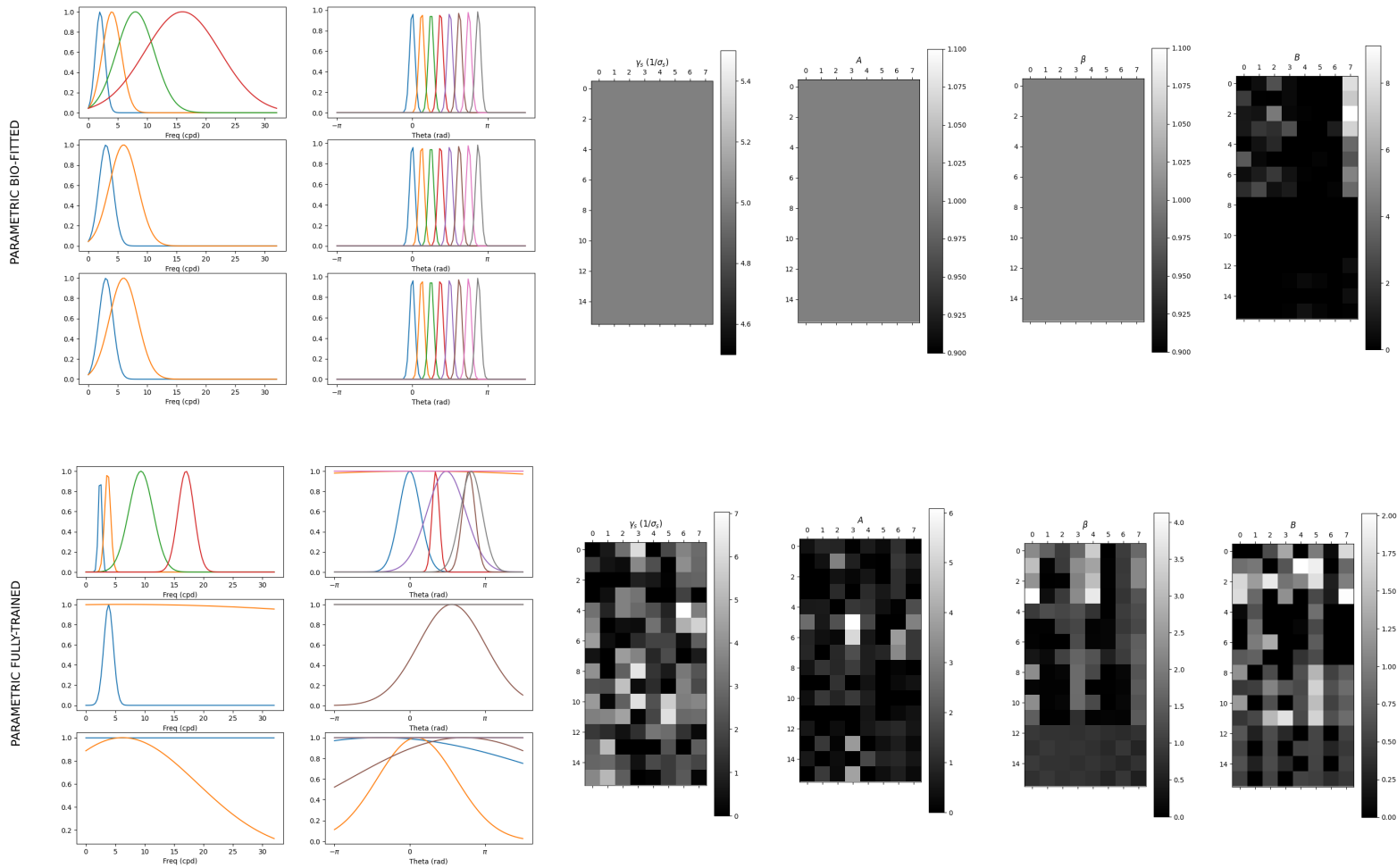


Fig. 11: Bandwidths (or tuning curves) in frequency and orientation of Gabor filters [left] together with the parameters of cortical divisive normalization [right]. Each row shows the parameters for each of the parametric models. The first column shows the relations for each frequency with regard their frequential neighbours. The second row shows the same but in orientation. Columns 3-7 shows the remainder parameters (γ , A , β , and B) for each of the 128 channels.

original non-parametric PerceNet, we have greatly restricted the formulation of the divisive normalization. Restricting the freedom of these layers prevents capturing all the richness of known biological behavior.

In the model with parametric formulation, this limitation is easily solvable if, instead of using this restricted formulation of divisive normalization, we complicate this expression a bit more and consider, as shown in the lower panel of Figure 12, more complex expressions of divisive normalization, or ones that include variations of the interaction kernels between neurons in divisive normalization. For example, in the case of Figure 12 lower panel on the left, through a small modification of the divisive normalization expression, the crispening effect in luminosity can be reproduced. The central and right panels of the lower panel of Figure 12 show that, by introducing an attractive term in the normalization to which the response of opponent channel sensors is subjected, Krauskopf and Gegenfurtner's adaptation can be reproduced. This consideration of more general versions of divisive normalization

would easily reproduce known perceptual phenomena and improve the model through the traditional scientific method of complicating the model so that it captures or reproduces more complex phenomena.

In this sense, our approach in this work would be a first-order approximation, whose objective is simply to illustrate the problems we have mentioned, basically the feature spreading problem, but it wouldn't be difficult in future work to complicate the model and obtain a metric that includes effects of adaptation to luminosity and illumination changes.

Finally, we show in Figure 13 a much more interesting phenomenon: the fact that, as we anticipated above, the particular objective through which the models are being optimized - that is, maximizing correlation with observers' opinions in subjectively evaluated databases - is an objective that is too unrestricted to adequately constrain the models, and we will demonstrate this through a final illustration in which we use different objective to adjust the models. This objective is equivalent to adjusting the models to try to reproduce not

the subjective opinion of distances, but something much more restrictive: the joint responses of all neurons in the last layer, the cortical layer after divisive normalization, of a model of the human visual system.

The results of this experiment are shown in Figure 13. Where we show the receptive fields obtained in the lateral geniculate nucleus and in V1 through such objective. In the first panel of Figure 13, we observe the emergence of center-surround type receptive fields and low-frequency blobs in the achromatic, red-green, and blue-yellow channels.

In these two cases, the obtained receptive fields are not biologically plausible, but it is very interesting to observe the emergence of center-surround neurons and the appearance of sensors with low-frequency blobs for red-green and blue-yellow channels without having imposed them parametrically.

We see that Gabor filters of specific frequencies appear, even if the model is not parametric, and the sum of the Fourier transforms of these filters, these receptive fields, turn out to be joint bandpass filters where even the oblique effect is reproduced as in human contrast sensitivity functions. In other words, when a sufficiently restrictive objective is used, even if the model isn't parameterized, biologically plausible results are obtained. Why is this so? We conjecture that the emergence of certain characteristics from achieving a particular objective is a kind of inverse problem because, for example, in Fredholm's formulation, information is lost when integrating over a set of inputs to obtain an objective function.

Multiple versions of these input weights can result in the same value of the objective function, so recovering those weights that give rise to that output would be the inverse problem, and the solution to this inverse problem, classically known as the Fredholm integral problem, is an inherently ill-behaved problem that has infinite solutions. For this reason, if the objective is not sufficiently restrictive, it's impossible for biologically plausible characteristics to emerge, because biologically plausible characteristics represent a single solution within an infinite set of solutions that give rise to the same value of the objective function. And so this problem is unsolvable with an insufficiently restrictive objective function.

If, on the contrary, a more restrictive objective function of the reproduction type is proposed, i.e. a simulation of physiology, then the appropriate characteristics do emerge.

VII. FINAL REMARKS

Results of the experiments presented here show that the conventional non-parametric approach to solve the problem of image quality metric (with millions of parameters) lead to correlations with human opinion at test which are similar (and sometimes worse) than what is obtained with equivalent parametric models (with three orders of magnitude less parameters), when the parametric models are initialized with known facts of visual psychophysics. In fact both kinds of models (conventional non-parametric and the proposed parametric) achieve correlations with Mean Opinion Score bigger than (estimated) inter-observer correlation. This suggests that overfitting is hard to remove when the only optimization criterion is correlation. Optimizing other tasks evaluated by

simple scores (as suggested in [60] and investigated in [61], [120]) does not seem to avoid overfitting either. Nevertheless, it seem sensible that parametrization is the way to go in order to understand what is going on in each layer of (otherwise) equivalent models: while the conventional models suffer from what we have called the *feature-spreading problem* across the layers, the proposed parametric models at least are more explainable and checking if certain qualitative behaviors hold, is easier.

In our last experiment, sensible neurons for LGN and V1 emerge (and also lead to a satisfactory correlation with MOS) when fitting non-parametric models to the responses of a *simulated brain*. This suggests a non-surprising concept: conventional (non-parametric) deep-nets could also lead to interesting (human-like) metric models if one could fit their parameters to enough data (i.e. physiological measurements at different layers of the visual pathway). Some groups are working in fitting cortical DNs using that approach [90], [121]. However, those models have not been used in the image quality problem. Nevertheless, despite some interesting physiological databases are available [122] the problem of data uniformization and the appropriateness of the available data for the image quality problem is not trivial issue.

Therefore, according to the results presented here, we foresee four important avenues for further research:

- 1) **Improve models:** The model proposed here is of course far from perfect and there is a number of possible improvements. For instance, Fig. ?? shows obvious improvements in the front-end of the model that carries out adaptation to luminance and color. The model presented here does not include variable scaling of the photo-receptors according to changes in spectral illumination (i.e. Von-Kries adaptation [72], or the crispening effects pointed out by Whittle [123]), but only takes into account the Weber law. Moreover, it does not take into account subtractive color adaptation in the opponent channels [124], [125]. This would imply more general versions of the DN, as shown in the figure. More importantly, it would require that the critical scaling of the nonlinear layers, the A 's in the presented notation, be input-dependent. Suggestions in this regard have already been given [65], and as suggested by Martinez et al. in their hand-crafted exploration, they could lead to better convergence of the models too. Another way to improve models is proposing new architectures where parameters are more independent in their influence to the goal. A possibility to do this is using the Amari's *natural gradient* concept [126]: combination of parameters in order to make them independent (by using PCA or ICA) would lead to equivalent architectures with less parameters, which eventually would have better convergence properties. The problem of dependence between parameters have been pointed out in this kind of retina-V1 models when using time-consuming experimental methods to psychophysically estimate the parameters [66]: Malo and Simoncelli shown that interaction between parameters of different layers increases the length of the experimental sessions that optimize one layer at a time. A

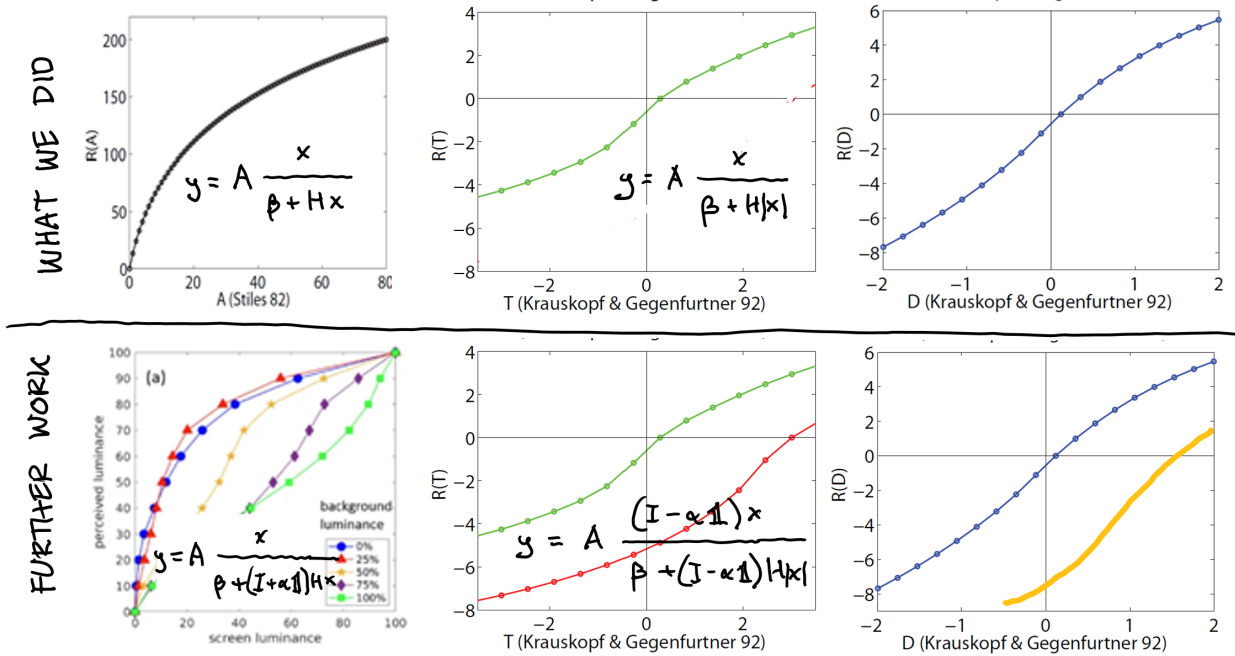


Fig. 12: Possible model improvements I Better luminance/color adaptation of the front end.

final new avenue to improve the presented architecture is connecting bio-inspired attention mechanisms (which basically work at the level of V1 of the presented architecture [127], [128]) with the attention mechanisms that are at the core of the current transformers [129].

- 2) **Optimize beyond correlation I: use classical psychophysics more extensively.** As pointed out in [130], the rich empirical literature on visual psychophysics that compiles critical facts that points out the inner workings of the visual system should be comprehensively taken into account, rather than just relying on fitting massive datasets that, given the dimensionality of the image space, may not represent (and hence may not impose) those critical facts in the models [65], [131]. In this regard, low-level [132], [133] and high-level [134] datasets have been compiled that could be used to this end. In particular, the low-level set includes 20 psychophysical experiments that exactly fit the facts associated to the layers of the model presented here. In the above experiment-based databases (as in the behavioral part of BrainScore) special care has to be put on how the qualitative behaviors are reproduced (or not) and how all the scores are combined for optimization. In this regard, in [65] they recommend loops in which regular optimization is alternated with qualitative check of the behavior. The prescription of going beyond correlation in massive databases is consistent with (more general) reports that suggest that conventional models optimized for too simple performance measures in reasonable visual tasks, behave in non-human ways [6], [135]–[139].

parameters: A problem of the classical literature in psychophysics is that it is thought just to point out behaviors (and that is totally fine), but in more quantitative (and parametric) models such as the ones considered here one needs to know specific values to initialize the unknowns, and these have to be valid for the whole range of features. For example, the available psychophysics that describes the interaction between Gabor channels, is too limited to fully constrain the models. In particular, classical results on cross-masking [24]–[27] do not consider all possible interactions between different spatio-temporal frequencies, orientation bands and chromatic content. Therefore, while these behaviors have been *heuristically* to improve a number of image processing tasks beyond image quality assessment⁴, specific values of these interactions are not available in the literature, and (as we saw here) if initializations are not close to the correct values it is very easy to end with wrong results after optimization. This means that new measurements following the classical psychophysical paradigms are still needed in the image quality application.

- 4) **Optimize beyond correlation II: use more recent psychophysics to decide between competing models (or parameters).** A feasible possibility to improve the optimization is including human observers in the loop. Recently, computation of adversarial images (images with maximum or minimum distortion for a certain metric) have been proposed as a simple methods so that a human observer can decide between competing metrics (or vision models). Note that for (overfitted)

- 3) **Extend classical data for extra constraint of pa-**

⁴Image coding [140]–[146], motion estimation [147], [148], video coding [149], [150], image denoising [151], image segmentation [152], [153], and classification [154], [155].

deep-metrics large distortions for the metric can actually be invisible to humans and small distortions for the metric can be highly visible for humans. This sort of *adversarial attacks* can be obtained using Maximum differentiation [35], [66], [103], [156] and related methods [157]. Detection of this sort of adversarial attacks via humans can be important to achieve more robust metrics,

In conclusion, this work presents a strong case for the use of parametric, human-inspired models in image quality assessment. By leveraging biological insights, we have shown that it is possible to build efficient, interpretable models that achieve competitive results with fewer parameters. This approach not only has implications for practical applications but also opens up new research directions in the field of computational modeling of the human visual system. Further exploration of how to balance performance with biological accuracy will be key to advancing both fields.

ACKNOWLEDGMENTS

This work was supported in part by MICIIN/FEDER/UE under Grant PID2020-118071GB-I00 and PDC2021-121522-C21, in part by Spanish MIU under Grant FPU21/02256 and in part by Generalitat Valenciana under Projects GV/2021/074, CIPROM/2021/056 and CIAPOT/2021/9. Some computer resources were provided by Artemisa, funded by the European Union ERDF and Comunitat Valenciana as well as the technical support provided by the Instituto de Física Corpuscular, IFIC (CSIC-UV). This work has been partially funded by the grant BBVA Foundations of Science program: Mathematics, Statistics, Computational Sciences and Artificial Intelligence (VIS4NN).

DATA AND CODE AVAILABILITY STATEMENT

Everything needed to reproduce the results obtained can be found in the following Github repository: <https://github.com/Jorgvt/paramperceptnet>.

REFERENCES

- [1] F. Campbell and J. Robson, "Application of Fourier analysis to the visibility of gratings," *Journal of Physiology*, vol. 197, pp. 551–566, 1968.
- [2] K. T. Mullen, "The CSF of human colour vision to red-green and yellow-blue chromatic gratings," *J. Physiol.*, vol. 359, pp. 381–400, 1985.
- [3] D. Cai, G. DeAngelis, and R. Freeman, "Spatiotemporal receptive field organization in the lateral geniculate nucleus of cats and kittens," *J. Neurophysiol.*, vol. 78, no. 2, pp. 1045–1061, 1997.
- [4] R. Shapley and M. J. Hawken, "Color in the cortex: single- and double-opponent cells," *Vision Research*, vol. 51, no. 7, pp. 701–717, 2011, vision Research 50th Anniversary Issue: Part 1. [Online]. Available: <https://www.sciencedirect.com/science/article/pii/S0042698911000526>
- [5] J. J. Atick, Z. Li, and A. N. Redlich, "Understanding retinal color coding from first principles," *Neural Computation*, vol. 4, no. 4, pp. 559–572, 1992.
- [6] Q. Li, A. Gomez-Villa, M. Bertalmío, and J. Malo, "Contrast sensitivity functions in autoencoders," *Journal of Vision*, vol. 22, no. 6, 2022.
- [7] J. Mannos and D. Sakrison, "The effects of a visual fidelity criterion of the encoding of images," *IEEE Transactions on Information Theory*, vol. 20, no. 4, pp. 525–536, 1974.
- [8] L. M. Hurvich and D. Jameson, "An opponent-process theory of color vision," *Psychological review*, vol. 64, Part 1 6, pp. 384–404, 1957.

- [9] D. H. Hubel, T. N. Wiesel *et al.*, "Receptive fields of single neurones in the cat's striate cortex," *J. Physiol.*, vol. 148, no. 3, pp. 574–591, 1959.
- [10] D. H. Hubel and T. N. Wiesel, "Integrative action in the cat's lateral geniculate body," *The Journal of physiology*, vol. 155, no. 2, p. 385, 1961.
- [11] C. Blakemore and F. Campbell, "On the existence of neurons selectivity sensitive to the orientation and size of retinal images," *J. Physiol.*, vol. 203, p. 237–260, 1969.
- [12] E. Simoncelli, W. Freeman, E. Adelson, and D. Heeger, "Shiftable multiscale transforms," *IEEE Trans. Inf. Theory*, vol. 38, no. 2, pp. 587–607, 1992.
- [13] B. Olshausen and D. Field, "Emergence of simple-cell receptive field properties by learning a sparse code for natural images," *Nature*, vol. 281, pp. 607–609, 1996.
- [14] A. Watson, "Perceptual-components architecture for digital video," *Journal of the Optical Society of America A*, vol. 7, no. 10, pp. 1943–1954, 1990.
- [15] K. Naka and W. Rushton, "S-potentials from colour units in the retina of fish (cyprinidae)," *J. Physiol.*, vol. 185, no. 3, pp. 536–555, 1966.
- [16] G. Legge and J. Foley, "Contrast masking in human vision," *Journal of the Optical Society of America*, vol. 70, pp. 1458–1471, 1980.
- [17] G. Legge, "A power law for contrast discrimination," *Vision Research*, vol. 18, pp. 68–91, 1981.
- [18] S. S. Haykin, *Neural networks and learning machines*, 3rd ed. Pearson Education, 2009.
- [19] I. Goodfellow, Y. Bengio, and A. Courville, *Deep Learning*. MIT Press, 2016, <http://www.deeplearningbook.org>.
- [20] P. Barten, "Evaluation of subjective image quality with the square root integral method," *Journal of the Optical Society of America A*, vol. 7, no. 10, pp. 2024–2031, 1990.
- [21] A. Ahumada, "Computational image quality metrics: A review," in *Intl. Symp. Dig. of Tech. Papers, Sta. Ana CA*, ser. Proceedings of the SID, J. Morreale, Ed., vol. 25, 1993, pp. 305–308.
- [22] S. Daly, "Application of a noise-adaptive Contrast Sensitivity Function to image data compression," *Optical Engineering*, vol. 29, no. 8, pp. 977–987, 1990.
- [23] A. Watson *et al.*, *Digital Images and Human Vision*. Massachusetts: MIT Press, 1993.
- [24] J. Ross, H. D. Speed, and F. W. Campbell, "Contrast adaptation and contrast masking in human vision," *Proceedings of the Royal Society of London. Series B: Biological Sciences*, vol. 246, no. 1315, pp. 61–70, 1991.
- [25] J. M. Foley, "Human luminance pattern-vision mechanisms: masking experiments require a new model," *J. Opt. Soc. Am. A*, vol. 11, no. 6, pp. 1710–1719, Jun 1994.
- [26] G. M. Boynton and J. M. Foley, "Temporal sensitivity of human luminance pattern mechanisms determined by masking with temporally modulated stimuli," *Vision Research*, vol. 39, no. 9, pp. 1641–1656, 1999. [Online]. Available: <https://www.sciencedirect.com/science/article/pii/S0042698998001990>
- [27] M. Morgan, C. Chubb, and J. Solomon, "Predicting the motion after-effect from sensitivity loss," *Vision Research*, vol. 46, no. 15, pp. 2412–2420, 2006.
- [28] H. R. Wilson and J. D. Cowan, "A mathematical theory of the functional dynamics of cortical and thalamic nervous tissue," *Kybernetik*, vol. 13, no. 2, pp. 55–80, Sep 1973.
- [29] S. Grossberg, "Contour enhancement, short-term memory, and constancies in reverberating neural networks," *Studies in Applied Mathematics*, vol. 52, pp. 213–257, 1973.
- [30] S.-i. Amari, "Dynamics of pattern formation in lateral-inhibition type neural fields," *Biological Cybernetics*, vol. 27, no. 2, pp. 77–87, Jun 1977.
- [31] D. J. Heeger, "Normalization of cell responses in cat striate cortex," *Visual Neuroscience*, vol. 9, no. 2, p. 181–197, 1992.
- [32] M. Carandini and D. Heeger, "Summation and division by neurons in visual cortex," *Science*, vol. 264, no. 5163, pp. 1333–6, 1994.
- [33] A. B. Watson and J. A. Solomon, "Model of visual contrast gain control and pattern masking," *J. Opt. Soc. Am. A*, vol. 14, no. 9, pp. 2379–2391, Sep 1997.
- [34] M. Carandini and D. J. Heeger, "Normalization as a canonical neural computation," *Nature Reviews Neuroscience*, vol. 13, no. 1, pp. 51–62, Jan. 2012, number: 1 Publisher: Nature Publishing Group. [Online]. Available: <https://www.nature.com/articles/nrn3136>
- [35] M. Martinez, P. Cyriac, T. Batard, M. Bertalmío, and J. Malo, "Derivatives and inverse of cascaded linear+nonlinear neural models,"

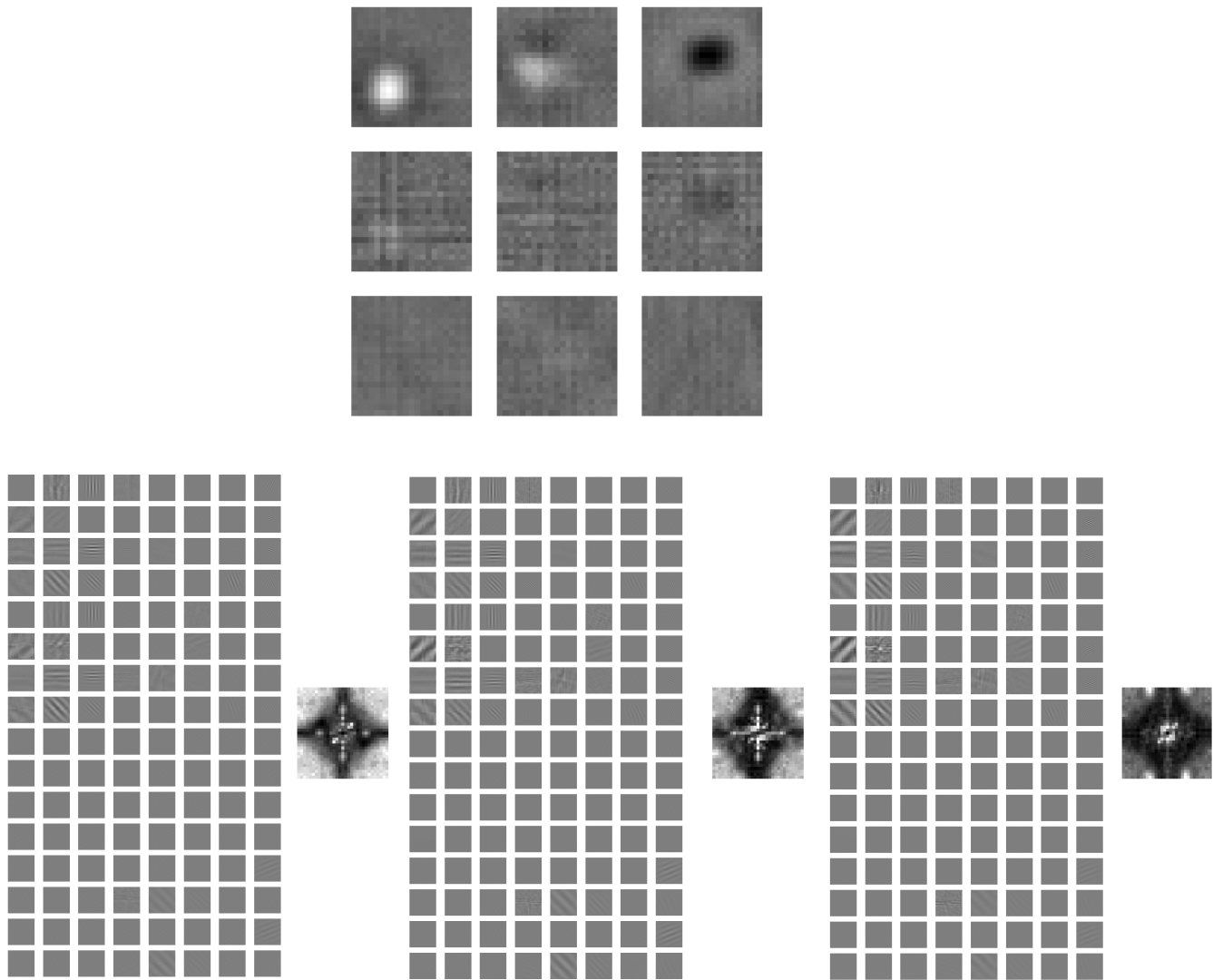


Fig. 13: **Possible model improvement II (third item in the final remarks)** Use goal functions and data that actually constrain the model. Here fitting simulated physiology. As explained in the text, obtaining the parameters is an inverse problem that may be ill posed. Fredholm Integral.

- PLOS ONE*, vol. 13, no. 10, pp. 1–49, 10 2018. [Online]. Available: <https://doi.org/10.1371/journal.pone.0201326>
- [36] S. Grossberg, “Behavioral contrast in short-term memory: Serial binary memory models or parallel continuous memory models?” *Journal of Mathematical Psychology*, vol. 3, pp. 199–219, 1978.
- [37] J. Malo, J. J. E. Taboada, and M. Bertalmío, “Cortical divisive normalization from wilson-cowan neural dynamics,” *J. Nonlinear Sci.*, vol. 34, no. 2, p. 35, 2024.
- [38] P. Teo and D. Heeger, “Perceptual image distortion,” *Proceedings of the SPIE*, vol. 2179, pp. 127–141, 1994.
- [39] J. Malo, A. Pons, and J. Artigas, “Subjective image fidelity metric based on bit allocation of the human visual system in the DCT domain,” *Image & Vision Computing*, vol. 15, no. 7, pp. 535–548, 1997.
- [40] A. Pons, J. Malo, J. Artigas, and P. Capilla, “Image quality metric based on multidimensional contrast perception models,” *Displays*, vol. 20, pp. 93–110, 1999.
- [41] A. B. Watson and J. Malo, “Video quality measures based on the standard spatial observer,” in *IEEE Proc. Int. Conf. Im. Proc.*, vol. 3, 2002, pp. III–III.
- [42] V. Laparra, J. Muñoz Marí, and J. Malo, “Divisive normalization image quality metric revisited,” *JOSA A*, vol. 27, no. 4, pp. 852–864, 2010.
- [43] V. Laparra, J. Ballé, A. Berardino, and E. P. Simoncelli, “Perceptual image quality assessment using a normalized laplacian pyramid,” in *Proc. IS&T Int’l Symposium on Electronic Imaging, Conf on Human Vision and Electronic Imaging (HVEI)*, B. Rogowitz, T. N. Pappas, and H. de Ridder, Eds., no. 16. San Francisco, CA: Society for Imaging Science and Technology, 14–18 Feb 2016, pp. 1–6.
- [44] V. Laparra, A. Berardino, J. Ballé, and E. P. Simoncelli, “Perceptually optimized image rendering,” *J. Opt. Soc. Am. A*, vol. 34, no. 9, pp. 1511–1525, Sep 2017. [Online]. Available: <https://opg.optica.org/josaa/abstract.cfm?URI=josaa-34-9-1511>
- [45] H. Barlow, “Sensory mechanisms, the reduction of redundancy, and intelligence,” *Proc. of the Nat. Phys. Lab. Symposium on the Mechanization of Thought Process*, no. 10, pp. 535–539, 1959.
- [46] —, “Redundancy reduction revisited,” *Network: Computation in Neural Systems*, vol. 12, pp. 241–253, 2001.
- [47] Z. Wang, A. C. Bovik, H. R. Sheikh, and E. P. Simoncelli, “Image quality assessment: From error visibility to structural similarity,” *IEEE Transactions on Image Processing*, vol. 13, no. 4, pp. 600–612, 2004.
- [48] —, “Perceptual image quality assessment: From error visibility to structural similarity,” *IEEE Trans Image Processing*, vol. 13, no. 4, pp. 600–612, 2004.
- [49] A. K. Moorthy and A. C. Bovik, “Blind image quality assessment: From natural scene statistics to perceptual quality,” *IEEE Transactions*

- on *Image Processing*, vol. 20, no. 12, pp. 3350–3364, 2011.
- [50] M. A. Saad, A. C. Bovik, and C. Charrier, “Blind image quality assessment: A natural scene statistics approach in the dct domain,” *IEEE Transactions on Image Processing*, vol. 21, no. 8, pp. 3339–3352, 2012.
- [51] O. Schwartz and E. P. Simoncelli, “Natural signal statistics and sensory gain control,” *Nature Neuroscience*, vol. 4, no. 8, pp. 819–825, Aug. 2001, number: 8 Publisher: Nature Publishing Group. [Online]. Available: https://www.nature.com/articles/nn0801_819
- [52] J. Malo and V. Laparra, “Psychophysically tuned divisive normalization approximately factorizes the pdf of natural images,” *Neural computation*, vol. 22, no. 12, pp. 3179–3206, 2010.
- [53] J. Malo, “Spatio-chromatic information available from different neural layers via gaussianization,” *The Journal of Mathematical Neuroscience*, vol. 10, no. 18, 2020.
- [54] H. Sheikh, A. Bovik, and G. de Veciana, “An information fidelity criterion for image quality assessment using natural scene statistics,” *IEEE Transactions on Image Processing*, vol. 14, no. 12, pp. 2117–2128, 2005.
- [55] H. Sheikh and A. Bovik, “Image information and visual quality,” *IEEE Transactions on Image Processing*, vol. 15, no. 2, pp. 430–444, 2006.
- [56] J. Malo, B. Kheravdar, and Q. Li, “Visual information fidelity with better vision models and better mutual information estimates,” *Journal of Vision*, vol. 21, no. 9, p. 2351, 2021.
- [57] A. Gomez-Villa, M. Bertalmío, and J. Malo, “Visual information flow in Wilson–Cowan networks,” *Journal of Neurophysiology*, vol. 123, no. 6, pp. 2249–2268, 2020.
- [58] J. Malo, J. Esteve-Taboada, G. Aguilar, M. Maertens, and F. Wichmann, “Estimating the contribution of early and late noise in vision from psychophysical data.” *Accepted in J. of Vision, preprint <https://arxiv.org/abs/2012.06608>*, 2024.
- [59] N. Ponomarenko, V. Lukin, A. Zelensky, K. Egiazarian, M. Carli, and F. Battisti, “Tid2008-a database for evaluation of full-reference visual quality assessment metrics,” vol. 10, no. 4, pp. 30–45, 2009.
- [60] R. Zhang, P. Isola, A. A. Efros, E. Shechtman, and O. Wang, “The unreasonable effectiveness of deep features as a perceptual metric,” *CoRR*, vol. abs/1801.03924, 2018. [Online]. Available: <http://arxiv.org/abs/1801.03924>
- [61] M. Kumar, N. Houlsby, N. Kalchbrenner, and E. D. Cubuk, “Do better imagenet classifiers assess perceptual similarity better?” *Trans. Mach. Learn. Res.*, 2022. [Online]. Available: <https://openreview.net/forum?id=qrGKGZZvH0>
- [62] P. Hernández-Cámara, J. Vila-Tomás, V. Laparra, and J. Malo, “Dissecting the effectiveness of deep features as a perceptual metric,” *Submitted to Neural Networks, Preprint SSRN: <http://dx.doi.org/10.2139/ssrn.4609207>*, 2024.
- [63] A. Hepburn, V. Laparra, J. Malo, R. McConville, and R. Santos-Rodríguez, “Perceptnet: A human visual system inspired neural network for estimating perceptual distance,” in *IEEE ICIP*, 2020, pp. 121–125.
- [64] G. “Shakhnarovich, D. Batra, B. Kulis, and K. Weinberger, “beyond mahalalanobis: supervised large-scale learning of similarity,” in *NIPS Workshop on Metric Learning*”, “2011”.
- [65] M. Martínez, M. Bertalmío, and J. Malo, “In praise of artifice reloaded: Caution with natural image databases in modeling vision,” *Front. Neurosci. doi: 10.3389/fnins.2019.00008*, 2019.
- [66] J. Malo and E. P. Simoncelli, “Geometrical and statistical properties of vision models obtained via maximum differentiation,” in *Human Vision and Electronic Imaging XX*, ser. Society of Photo-Optical Instrumentation Engineers (SPIE) Conference Series, B. E. Rogowitz, T. N. Pappas, and H. de Ridder, Eds., vol. 9394, Mar. 2015, p. 93940L.
- [67] J. Vila-Tomás, P. Hernández-Cámara, Q. Li, A. Hepburn, V. Laparra, and J. Malo, “Basic psychophysics of deep networks trained to reproduce subjective image distortion,” in *Workshop on Deep Learning in Vision Science at the Iberian Conference on Perception*, 2022.
- [68] J. Vila-Tomás, P. Hernández-Cámara, Q. Li, V. Laparra, and J. Malo, “A turing test for artificial nets devoted to model human vision,” 2025. [Online]. Available: <https://arxiv.org/abs/2502.00721>
- [69] N. Alabau-Bosque, P. Daudén-Oliver, J. Vila-Tomás, V. Laparra, and J. Malo, “Invariance of deep image quality metrics to affine transformations,” 2024. [Online]. Available: <https://arxiv.org/abs/2407.17927>
- [70] G. Wyszecki and W. Stiles, *Color Science: Concepts and Methods, Quantitative Data and Formulae*. New Jersey: John Wiley & Sons, 2000.
- [71] J. B. Demb and D. H. Brainard, *Neurons show their true colours*. Nature, 2010.
- [72] M. Fairchild, *Color Appearance Models*, ser. The Wiley-IS&T Series in Imaging Science and Technology. Wiley, 2013.
- [73] J. M. Hillis and D. H. Brainard, “Do common mechanisms of adaptation mediate color discrimination and appearance? uniform backgrounds,” *J. Opt. Soc. Am. A*, vol. 22, no. 10, pp. 2090–2106, Oct 2005.
- [74] A. Abrams, J. Hillis, and D. Brainard, “The relation between color discrimination and color constancy: when is optimal adaptation task dependent?” *Neural Comp.*, vol. 19, no. 10, 2007.
- [75] L. M. Hurvich and D. Jameson, “An opponent-process theory of color vision,” *Psychological review*, vol. 64, Part 1 6, pp. 384–404, 1957.
- [76] J. Vila-Tomás, P. Hernández-Cámara, and J. Malo, “Artificial psychophysics questions classical hue cancellation experiments,” *Frontiers in Neuroscience*, vol. 17, 2023.
- [77] J. Krauskopf and K. Gegenfurtner, “Color discrimination and adaptation,” *Vision Research*, vol. 32, no. 11, pp. 2165–2175, 1992.
- [78] J. Romero, J. A. García, L. J. del Barco, and E. Hita, “Evaluation of color-discrimination ellipsoids in two-color spaces,” *J. Opt. Soc. Am. A*, vol. 10, no. 5, pp. 827–837, May 1993. [Online]. Available: <https://opg.optica.org/josaa/abstract.cfm?URI=josaa-10-5-827>
- [79] V. Laparra, S. Jiménez, G. Camps-Valls, and J. Malo, “Nonlinearities and adaptation of color vision from Sequential Principal Curves Analysis,” *Neural Computation*, vol. 24, no. 10, 2012.
- [80] V. Laparra and J. Malo, “Visual aftereffects and sensory nonlinearities from a single statistical framework,” *Frontiers in Human Neuroscience*, vol. 9, p. 557, 2015. [Online]. Available: <http://journal.frontiersin.org/article/10.3389/fnhum.2015.00557>
- [81] J. Malo, “Characterization of HVS threshold performance by a weighting function in the Gabor domain,” *J. Mod. Opt.*, vol. 44, no. 1, pp. 127–148, 1997.
- [82] K. Louie and P. W. Glimcher, “Normalization principles in computational neuroscience,” 07 2019. [Online]. Available: <https://oxfordre.com/neuroscience/view/10.1093/acrefore/9780190264086.001.0001/acrefore-9780190264086-e-43>
- [83] R. Mantiuk, K. J. Kim, A. G. Rempel, and W. Heidrich, “Hdr-vdp-2: a calibrated visual metric for visibility and quality predictions in all luminance conditions,” *ACM Trans. Graph.*, vol. 30, no. 4, Jul. 2011. [Online]. Available: <https://doi.org/10.1145/2010324.1964935>
- [84] D. Hammou, L. Krasula, C. G. Bampis, Z. Li, and R. K. Mantiuk, “Image quality assessment across viewing distances: A comparison study of csf-based and rescaling-based metrics,” *Electronic Imaging*, vol. 36, no. 11, pp. 225–1–225–1, 2024. [Online]. Available: <https://library.imaging.org/ei/articles/36/11/HVEI-225>
- [85] A. Krizhevsky, I. Sutskever, and G. Hinton, “Imagenet classification with deep convolutional neural networks,” in *Advances in Neural Information Processing Systems*, F. Pereira, C. Burges, L. Bottou, and K. Weinberger, Eds., vol. 25. Curran Associates, Inc., 2012. [Online]. Available: https://proceedings.neurips.cc/paper_files/paper/2012/file/c399862d3b9d6b76c8436e924a68c45b-Paper.pdf
- [86] K. Simonyan and A. Zisserman, “Very deep convolutional networks for large-scale image recognition,” 2015. [Online]. Available: <https://arxiv.org/abs/1409.1556>
- [87] M. Ren, R. Liao, R. Urtasun, F. H. Sinz, and R. S. Zemel, “Normalizing the normalizers: Comparing and extending network normalization schemes,” *CoRR*, vol. abs/1611.04520, 2016.
- [88] L. G. S. Giraldo and O. Schwartz, “Integrating flexible normalization into midlevel representations of deep convolutional neural networks,” *Neural Computation*, vol. 31, pp. 2138–2176, 2019.
- [89] X. Pan, L. G. S. Giraldo, E. Kartal, and O. Schwartz, “Brain-inspired weighted normalization for cnn image classification,” *ICLR conference in bioRxiv*, 2021.
- [90] M. F. Burg, S. A. Cadena, G. H. Denfield, E. Y. Walker, A. S. Tolia, M. Bethge, and A. S. Ecker, “Learning divisive normalization in primary visual cortex,” *PLOS Computational Biology*, vol. 17, no. 6, p. e1009028, 2021.
- [91] A. Hepburn, V. Laparra, J. Malo, R. McConville, and R. Santos-Rodríguez, “PerceptNet: A Human Visual System Inspired Neural Network for Estimating Perceptual Distance,” in *2020 IEEE International Conference on Image Processing (ICIP)*, Oct. 2020, pp. 121–125, arXiv:1910.12548 [cs, eess, stat]. [Online]. Available: <http://arxiv.org/abs/1910.12548>
- [92] M. Krenn et al., “On scientific understanding with artificial intelligence,” *Nature Reviews Physics*, vol. 4, no. 12, pp. 761–769, 2016.
- [93] J. Ballé, V. Laparra, and E. Simoncelli, “Density modeling of images using a generalized normalization transformation,” Jan. 2016, 4th International Conference on Learning Representations, ICLR 2016 ; Conference date: 02-05-2016 Through 04-05-2016.

- [94] S. Luan *et al.*, “Gabor convolutional networks,” *CoRR*, vol. abs/1705.01450, 2017. [Online]. Available: <http://arxiv.org/abs/1705.01450>
- [95] A. Alekseev and A. Bobe, “Gabornet: Gabor filters with learnable parameters in deep convolutional neural networks,” *CoRR*, vol. abs/1904.13204, 2019.
- [96] J. Dapello, T. Marques, M. Schrimpf, F. Geiger, D. Cox, and J. J. DiCarlo, “Simulating a primary visual cortex at the front of cnns improves robustness to image perturbations,” in *Advances in Neural Information Processing Systems*, H. Larochelle, M. Ranzato, R. Hadsell, M. Balcan, and H. Lin, Eds., vol. 33. Curran Associates, Inc., 2020, pp. 13 073–13 087. [Online]. Available: https://proceedings.neurips.cc/paper_files/paper/2020/file/98b17f068d5d9b7668e19fb8ae470841-Paper.pdf
- [97] J. C. Pérez, M. Alfara, G. Jeanneret, A. Bibi, A. K. Thabet, B. Ghanem, and P. Arbeláez, “Robust gabor networks,” *CoRR*, vol. abs/1912.05661, 2019. [Online]. Available: <http://arxiv.org/abs/1912.05661>
- [98] V. Veerabadran, R. Raina, and V. R. de Sa, “Bio-inspired learnable divisive normalization for ANNs,” in *SVRHM 2021 Workshop @ NeurIPS*, 2021. [Online]. Available: <https://openreview.net/forum?id=-ZojASLOsrV>
- [99] Z. Babaiee, R. M. Hasani, M. Lechner, D. Rus, and R. Grosu, “On-off center-surround receptive fields for accurate and robust image classification,” *CoRR*, vol. abs/2106.07091, 2021. [Online]. Available: <https://arxiv.org/abs/2106.07091>
- [100] B. D. Evans, G. Malhotra, and J. S. Bowers, “Biological convolutions improve dnn robustness to noise and generalisation,” *Neural Networks*, vol. 148, pp. 96–110, 2022.
- [101] Q. Chen, C. Li, J. Ning, S. Lin, and K. He, “Gmconv: Modulating effective receptive fields for convolutional kernels,” 2023. [Online]. Available: <https://arxiv.org/abs/2302.04544>
- [102] V. Bonin, V. Mante, and M. Carandini, “The suppressive field of neurons in lateral geniculate nucleus,” *The Journal of Neuroscience*, vol. 25(47), pp. 10 844 – 10 856, 2005.
- [103] Z. Wang and E. P. Simoncelli, “Maximum differentiation (mad) competition: A methodology for comparing computational models of perceptual quantities,” *Journal of Vision*, vol. 8, no. 12, pp. 8–8, 09 2008. [Online]. Available: <https://doi.org/10.1167/8.12.8>
- [104] Z. Wang and A. C. Bovik, *Modern Image Quality Assessment*, ser. Synthesis Lectures on Image, Video, and Multimedia Processing. Morgan & Claypool Publishers, 2006. [Online]. Available: <https://doi.org/10.2200/S00010ED1V01Y200508IVM003>
- [105] N. Ponomarenko, V. Lukin, A. Zelensky, K. Egiazarian, J. Astola, M. Carli, and F. Battisti, “TID2008 – A Database for Evaluation of Full-Reference Visual Quality Assessment Metrics,” 2009.
- [106] N. Ponomarenko, L. Jin, O. Ieremeiev, V. Lukin, K. Egiazarian, J. Astola, B. Vozel, K. Chehdi, M. Carli, F. Battisti, and C.-C. Jay Kuo, “Image database TID2013: Peculiarities, results and perspectives,” *Signal Processing: Image Communication*, vol. 30, pp. 57–77, Jan. 2015. [Online]. Available: <https://linkinghub.elsevier.com/retrieve/pii/S0923596514001490>
- [107] H. Lin, V. Hosu, and D. Saupe, “Kadid-10k: A large-scale artificially distorted iqa database,” in *2019 Tenth International Conference on Quality of Multimedia Experience (QoMEX)*. IEEE, 2019, pp. 1–3.
- [108] L. Martínez, M. Molano-Mazón, X. Wang, F. Sommer, and J. Hirsch, “Statistical wiring of thalamic receptive fields optimizes spatial sampling of the retinal image”. *Neuron*.
- [109] J. Lindsey, S. A. Ocko, S. Ganguli, and S. Deny, “The effects of neural resource constraints on early visual representations,” in *International Conference on Learning Representations*, 2019. [Online]. Available: <https://openreview.net/forum?id=S1xq3oR5tQ>
- [110] J. Malo, A. Pons, and J. Artigas, “Subjective image fidelity metric based on bit allocation of the human visual system in the dct domain,” *Image and Vision Computing*, vol. 15, no. 7, pp. 535–548, 1997. [Online]. Available: <https://www.sciencedirect.com/science/article/pii/S0262885696000042>
- [111] “True color kodak images,” accessed: 2025-02-11.
- [112] J. G. Daugman, “Spatial visual channels in the fourier plane,” *Vision Research*, vol. 24, no. 9, pp. 891–910, 1984. [Online]. Available: <https://www.sciencedirect.com/science/article/pii/0042698984900658>
- [113] G. T. Fechner, “Elements of psychophysics,” *Breitkopf und Härtel*, 1860.
- [114] V. Mante, R. A. Frazor, V. Bonin, W. S. Geisler, and M. Carandini, “Independence of luminance and contrast in natural scenes and in the early visual system,” *Nature Neuroscience*, 2005.
- [115] E. Peli, “Contrast in complex images,” *JOSA A*, vol. 7, pp. 2032–2040, 1990.
- [116] J. Malo and M. Luque, “ColorLab: A Matlab Toolbox for Color Science and Calibrated Color Image Processing,” *Univ. Valencia*. https://isp.uv.es/code/vision_and_color/colorlab/content/, 2002. [Online]. Available: https://isp.uv.es/code/vision_and_color/colorlab/content/
- [117] J. Malo and J. Gutierrez, “VistaLab: The Matlab toolbox for linear spatio-temporal Vision Models,” *Univ. Valencia*. https://isp.uv.es/code/vision_and_color/colorlab/vistalab/, 2002. [Online]. Available: https://isp.uv.es/code/vision_and_color/colorlab/vistalab/
- [118] J. Daugman, “Entropy reduction and decorrelation in visual coding by oriented neural receptive fields,” *IEEE Transactions on Biomedical Engineering*, vol. 36, pp. 107–114, 1989.
- [119] A. Watson, “Efficiency of a model human image code,” *Journal of Optical Society of America A*, vol. 4, no. 12, pp. 2401–2417, 1987.
- [120] P. Hernández-Cámara, J. Vila-Tomás, V. Laparra, and J. Malo, “Dissecting the effectiveness of deep features as metric of perceptual image quality,” *Neural Networks*, vol. 185, p. 107189, 2025. [Online]. Available: <https://www.sciencedirect.com/science/article/pii/S0893608025000681>
- [121] S. A. Cadena, G. H. Denfield, E. Y. Walker, L. A. Gatys, A. S. Tolia, M. Bethge, and A. S. Ecker, “Deep convolutional models improve predictions of macaque v1 responses to natural images,” *PLOS Computational Biology*, vol. 15, no. 4, pp. 1–27, 04 2019. [Online]. Available: <https://doi.org/10.1371/journal.pcbi.1006897>
- [122] M. Schrimpf, J. Kubilius, H. Hong, N. J. Majaj, R. Rajalingham, E. B. Issa, K. Kar, P. Bashivan, J. Prescott-Roy, F. Geiger, K. Schmidt, D. L. K. Yamins, and J. J. DiCarlo, “Brain-score: Which artificial neural network for object recognition is most brain-like?” *bioRxiv preprint*, 2018. [Online]. Available: <https://www.biorxiv.org/content/10.1101/407007v2>
- [123] P. Whittle, “Brightness, discriminability and the “crispness effect”,” *Vision Research*, vol. 32, no. 8, pp. 1493–1507, 1992. [Online]. Available: <https://www.sciencedirect.com/science/article/pii/004269899290205W>
- [124] J. Krauskopf and G. Karl, “Color discrimination and adaptation,” *Vision Research*, vol. 32, no. 11, pp. 2165–2175, 1992. [Online]. Available: <https://www.sciencedirect.com/science/article/pii/004269899290077V>
- [125] M. U. Gutmann, V. Laparra, A. Hyvärinen, and J. Malo, “Spatio-chromatic adaptation via higher-order canonical correlation analysis of natural images,” *PLoS ONE*, vol. 9, no. 2, p. e86481, 2014.
- [126] S.-i. Amari, “Natural Gradient Works Efficiently in Learning.”
- [127] L. Itti, C. Koch, and E. Niebur, “A model of saliency-based visual attention for rapid scene analysis,” *IEEE Transactions on Pattern Analysis and Machine Intelligence*, vol. 20, no. 11, pp. 1254–1259, 1998.
- [128] Z. Li, “A saliency map in primary visual cortex,” *Trends in Cognitive Sciences*, vol. 6, no. 1, pp. 9–16, 2002.
- [129] A. Vaswani, N. Shazeer, N. Parmar, J. Uszkoreit, L. Jones, A. N. Gomez, L. Kaiser, and I. Polosukhin, “Attention Is All You Need,” Dec. 2017, arXiv:1706.03762 [cs]. [Online]. Available: <http://arxiv.org/abs/1706.03762>
- [130] J. S. Bowers, G. Malhotra, M. Dujmović, M. L. Montero, C. Tsvetkov, V. Biscione, G. Puebla, F. Adolfi, J. E. Hummel, R. F. Heaton *et al.*, “Deep problems with neural network models of human vision,” *Behavioral and Brain Sciences*, vol. 46, p. e385, 2023.
- [131] N. Rust and J. Movshon, “In praise of artifice,” *Nature Neurosci.*, vol. 8, no. 12, pp. 1647–1650, 2005.
- [132] J. Malo and J. Bowers, “The low-level mindset: compelling low-level visual psychophysics to evaluate image computable vision models,” Invited talk, Psychol. Dept. University of Bristol, 2024.
- [133] J. Vila-Tomás, P. Hernández-Cámara, Q. Li, V. Laparra, and J. Malo, “A Turing test for Artificial nets devoted to model Human vision,” *arXiv preprint arXiv:2502.00721*, 2025.
- [134] V. Biscione, D. Yin, G. Malhotra, M. Dujmovic, M. L. Montero, G. Puebla, F. Adolfi, R. F. Heaton, J. E. Hummel, B. D. Evans *et al.*, “Mindset: Vision. a toolbox for testing dnns on key psychological experiments,” *arXiv preprint arXiv:2404.05290*, 2024.
- [135] R. Geirhos, K. Meding, and F. A. Wichmann, “Beyond accuracy: quantifying trial-by-trial behaviour of cnns and humans by measuring error consistency,” *CoRR*, vol. abs/2006.16736, 2020. [Online]. Available: <https://arxiv.org/abs/2006.16736>
- [136] R. Geirhos, P. Rubisch, C. Michaelis, M. Bethge, F. A. Wichmann, and W. Brendel, “Imagenet-trained cnns are biased towards texture; increasing shape bias improves accuracy and robustness,” *CoRR*, vol.

abs/1811.12231, 2018. [Online]. Available: <http://arxiv.org/abs/1811.12231>

- [137] A. Akbarinia, Y. Morgenstern, and K. R. Gegenfurtner, “Contrast sensitivity function in deep networks,” *bioRxiv*, 2023.
- [138] A. Gomez-Villa, A. Martin, J. Vazquez, M. Bertalmio, and J. Malo, “Color illusions also deceive CNNs for low-level vision tasks: Analysis and implications,” *Vision Research*, vol. 176, pp. 156–174, 2020.
- [139] P. Hernández-Cámara, J. Vila-Tomás, V. Laparra, and J. Malo, “Dissecting the effectiveness of deep features as metric of perceptual image quality,” *Neural Networks*, vol. 185, p. 107189, 2025. [Online]. Available: <https://www.sciencedirect.com/science/article/pii/S0893608025000681>
- [140] J. Malo, A. Pons, and J. Artigas, “Bit allocation algorithm for codebook design in vector quantization fully based on human visual system non-linearities for suprathreshold contrasts,” *Electronics Letters*, vol. 31, no. 15, pp. 1229–1231, 1995.
- [141] J. Malo, F. Ferri, J. Albert, and J. Soret, “Comparison of perceptually uniform quantization with average error minimization in image transform coding,” *Electronics Letters*, vol. 35, no. 13, pp. 1067–1068, 1999.
- [142] J. Malo, F. Ferri, J. Albert, J. Soret, and J. Artigas, “The role of perceptual contrast non-linearities in image transform coding,” *Image & Vision Computing*, vol. 18, no. 3, pp. 233–246, 2000.
- [143] D. Taubman and M. Marcellin, *JPEG2000 Image Compression Fundamentals, Standards and Practice*. Springer Publishing Company, Incorporated, 2013.
- [144] I. Epifanio, J. Gutiérrez, and J. Malo, “Linear transform for simultaneous diagonalization of covariance and perceptual metric matrix in image coding,” *Pattern Recognition*, vol. 36, pp. 1799–1811, 2003.
- [145] J. Malo, I. Epifanio, R. Navarro, and E. Simoncelli, “Non-linear image representation for efficient perceptual coding,” *IEEE Transactions on Image Processing*, vol. 15, no. 1, pp. 68–80, 2006.
- [146] G. Camps, J. Gutiérrez, G. Gómez, and J. Malo, “On the suitable domain for SVM training in image coding,” *JMLR*, vol. 9, pp. 49–66, 2008.
- [147] J. Malo, F. Ferri, J. Gutierrez, and I. Epifanio, “Importance of quantizer design compared to optimal multigrid motion estimation in video coding,” *Electronics Letters*, vol. 36, no. 9, pp. 507–509, 2000.
- [148] J. Malo, F. Ferri, J. Albert, and J. Artigas, “Splitting criterion for hierarchical motion estimation based on perceptual coding,” *Electronics Letters*, vol. 34, no. 6, pp. 541–543, 1998.
- [149] J. Malo, J. Gutierrez, I. Epifanio, F. Ferri, and J. M. Artigas, “Perceptual feed-back in multigrid motion estimation using an improved DCT quantization,” *IEEE Transactions on Image Processing*, vol. 10, no. 10, pp. 1411–1427, 2001.
- [150] J. Malo, J. Gutierrez, I. Epifanio, and F. Ferri, “Perceptually weighted optical flow for motion-based segmentation in MPEG-4 paradigm,” *Electronics Letters*, vol. 36, no. 20, pp. 1693–1694, 2000.
- [151] J. Gutiérrez, F. Ferri, and J. Malo, “Regularization operators for natural images based on nonlinear perception models,” *IEEE Tr. Im. Proc.*, vol. 15, no. 1, pp. 189–200, 2006.
- [152] P. Hernández-Cámara, J. Vila-Tomás, V. Laparra, and J. Malo, “Neural networks with divisive normalization for image segmentation,” *Pattern Recognition Letters*, vol. 173, pp. 64–71, 2023. [Online]. Available: <https://www.sciencedirect.com/science/article/pii/S0167865523002209>
- [153] P. Hernández-Cámara, J. Vila-Tomás, P. Dauden-Oliver, N. Alabau-Bosque, V. Laparra, and J. Malo, “Image segmentation via divisive normalization: dealing with environmental diversity,” 2024. [Online]. Available: <https://arxiv.org/abs/2407.17829>
- [154] R. Coen-Cagli and O. Schwartz, “The impact on midlevel vision of statistically optimal divisive normalization in v1,” *Journal of Vision*, vol. 13, no. 8, pp. 13–13, 07 2013. [Online]. Available: <https://doi.org/10.1167/13.8.13>
- [155] M. Miller, S. Chung, and K. D. Miller, “Divisive feature normalization improves image recognition performance in alexnet,” in *International Conference on Learning Representations*, 2022. [Online]. Available: <https://openreview.net/forum?id=aOX3a9q3RVV>
- [156] K. Ma, Z. Duanmu, Z. Wang, Q. Wu, W. Liu, H. Yong, H. Li, and L. Zhang, “Group maximum differentiation competition: Model comparison with few samples,” *IEEE Transactions on Pattern Analysis and Machine Intelligence*, vol. 42, no. 4, pp. 851–864, 2020.
- [157] T. Golan, P. C. Raju, and N. Kriegeskorte, “Controversial stimuli: Pitting neural networks against each other as models of human cognition,” *Proceedings of the National Academy of Sciences*, vol. 117, no. 47, pp. 29330–29337, 2020. [Online]. Available: <https://www.pnas.org/doi/abs/10.1073/pnas.1912334117>

APPENDIX A PARAMETRIC FORMULATIONS - OPTIONS

Options for the parametrization of the Gabor layer

The *Gabor* filter allows different degrees of restriction in the parametrization which involves different number of parameters:

- **All parameters free:** Generate $C_{in} \times C_{out}$ Gabor filters with different parameters for each of them. $\#Params = C_{in} \times C_{out} \times 5$.
- **Repeat for same inputs:** Generate C_{out} Gabor filters with different parameters for each of them and repeat them for every input channel, i.e. If we have 3 input channels and we want to output only 1 feature, we will only generate 1 Gabor and repeat it 3 times to make the convolution. $\#Params = C_{out} \times 5$.
- **Depthwise separable:** A variation of the previous one where the Gabor filter is repeated across the input channels but each one of them is weighted by a learned parameter A , multiplying the amount of parameters by a factor C_{in} . This is our selection which is consistent with the depthwise separable idea. $\#Params = C_{out} \times (5 + C_{in})$.
- **Fixed set of f and θ :** Define a set of f and θ and generate the Gabors corresponding to all their possible combinations ($N_f \times N_\theta$ filters). Each of them will have an independent Gaussian envelope. As before, each Gabor is repeated C_{in} times to perform the convolution. $\#Params = N_f + N_\theta + (N_f + N_\theta) \times 3$ (params of the gaussian) $= (N_f + N_\theta) \times 4$.
- **Fixed set of f and θ (Restricted envelope):** All the previous parametrizations allow the Gaussian envelopes to have their long side perpendicular to the sinusoid, but this is not what we find in humans. To enforce a more human-like structure we can parametrize $\sigma_y = 2\sigma_x$, reducing even more the amount of parameters. $\#Params = N_f + N_\theta + (N_f + N_\theta) \times 2$ (params of the gaussian) $= (N_f + N_\theta) \times 3$.

Options for the parametrization of the DN layer

We can employ different forms of the canonical Divisive Normalization (which corresponds to choosing different forms from the operator H). Keep in mind that the output of the Divisive Normalization has the same number of channels as the input ($z = i$).

- **Original:** Dense interaction between pixels and features. $\#Params = k_x \times k_y \times D_i \times D_o = k_x \times k_y \times D_i^2$, where k_x and k_y are the width and height of the convolutional filter respectively. This is the form to be found in the original PerceptNet model [91].
- **Spatial Gaussian:** Gaussian interaction between pixels and dense interaction between features.
 - **With repetition:** Defining C_{in} Gaussians and repeating over the C_{in} features. $\#Params = C_{in} \times 1$. (Remember that a Gaussian has only 1 parameter).
 - **Without repetition:** $\#Params = C_{in} \times C_{in} = C_{in}^2$.
- **Spatial-Features Gaussian:** Gaussian interaction between pixels and features. $\#Params = C_{in} \times C_{in} = C_{in}^2$.

- **Spatio-Temp-Orient Gaussian:** Gaussian interaction between pixels and features taking into account the features' frequencies and orientations. Requires that the frequencies and orientations of the input features are known (something that we get if using parametric Gabor layers as well). $\#Params = C_{in} \times N_f \times N_\theta$.

APPENDIX B MODEL DESCRIPTION IN DETAIL

- **Layer 1 (DN - "Von-Kries / Weber adaptation"):** it applies a gamma correction on the input. This layer mainly enhances low luminance ranges while compressing high luminance ranges following the idea in Weber law. In order to do so we use the divisive normalization (Sec III-B2) applied to each channel and each pixel independently (no interaction between pixels nor features). The parameters β and H are shared by the three channels, thus both β and H are scalar. Therefore this layer only has 2 parameters. H is restricted to only positive values with a clipping operation after each parameter update.
- **Layer 2 (Convolution - "Opponent Color Space"):** it is meant to reproduce the transformation to color opponent space. It is implemented as a convolution with 3 filters where each filter has spatial size 1×1 , providing 3 outputs where each one is a linear combination of the three inputs (RGB corrected values). Therefore the layer has 9 parameters. It is initialized to match the Jameson & Hurvich [] transformation to opponent color space. A spatial max pooling of 2×2 is applied.
- **Layer 3 (DN - "Krauskopf-Genenfurtner Adaptation") :** This layer is inspired by the Von Kries color adaptation and is applied via a divisive normalization. It acts independently on the three channels but the weights are not shared (as opposed to the first layer). There is no spatial interaction either. This means that β and H are scalar but different for each channel, leading to having 6 parameters (2 per input feature).
- **Layer 4 (Convolution - "LGN center-surround cells"):** applies a set of Center Surround receptive filters as seen in retina and the LGN []. This is implemented with a Difference of (Symmetric) Gaussians (DoG) (sec. III-B1b). We allow feature interaction in this layer, so we will need 9 DoGs (3 input channels \times 3 output channels), resulting in 18 parameters, 27 when considering A_z . Even though we allow feature interaction, it is initialized so that there is no interaction between the channels by choosing A_{i_o} accordingly. A spatial max pooling of 2×2 is applied.
- **Layer 5 (DN - "Generic energy contrast masking"):** Replicates the LGN normalization by applying a divisive normalization, where H is a parametric Gaussian kernel, independently to each input channel. As there are 3 input channels and a Gaussian can be parametrized by a single parameter σ , this layer has 9 parameters total considering the bias and the A_z coefficients.
- **Layer 6 (Convolution - "Gabor receptive fields in V1"):** Visual cortex (V1) simple cells modeled by applying the convolution operation between a set of para-

metric Gabor filters and the input. Each output channel corresponds to a specific frequency and orientation i.e. a different Gabor filter G . Mimicking the human visual system, we employ 64 filters for the achromatic channel and 32 for each of the chromatic channels. At initialization time the input channels don't mix, but this is controlled by a set of coefficients A_z that can vary and allow their mixture. Maintaining the human inspiration, the achromatic Gabor filters are combinations of 4 frequencies, 8 orientations and two phases, while the chromatic filters only have two possible frequencies. This results in having $(3 \times 4 + 2 \times 8) + 2 \times (3 \times 2 + 2 \times 8) = 72$ Gabor parameters and $3 \times 128 A_z$ coefficients, adding up to 456 parameters.

- **Layer 7 (DN - "Space/frequency/Orientation masking in V1"):** Divisive normalization in V1 that combines the outputs of the simple cells from the previous layer into complex cells. As the previous layer's filters are Gabors, we can define the denominator kernel so that there is a Gaussian relation between input features, taking into account not only the spatial position of the pixels but also the frequency and orientation of the features. Its expression is shown in Eq. 6. As we are considering only a reduced set of frequencies and orientations, we only need $4 + 2 + 2 = 8 \sigma_f$, and $8 \times 3 = 24 \sigma_\theta$ to express a Gaussian relation between scales and orientations. As there are 128 features we will use 128 σ_s , with their respective 128 A_z to model the spatial relation between pixels. The chromatic interaction is modelled with a 3×3 matrix H . Including the 128 biases and the 128 B coefficients, the number of parameters of this layer adds up to 553.

$$G(x, y, \Theta) = He^{-\frac{1}{2} \left(\frac{x^2 + y^2}{\sigma_s^2} + \frac{(f - f_0)^2}{\sigma_f^2} + \frac{(\theta - \theta_0)^2}{\sigma_\theta^2} \right)} \quad (6)$$

APPENDIX C PSYCHOPHYSICALLY MEANINGFUL INITIALIZATION

Following the ideas exposed in section ?? we set the parameters of each layer as described in table V. Central column in Figure 7 shows the effect of this choices in the parameters for the first 5 layers, the same for the layer 6 in Fig. 9, and layer 7 in Fig. 11. The effect of each layer over a natural image is shown in figures 5 and 6. Fig. 7 first row shows that the first layer enhances the sensitivity for low luminances and reduces it for high luminances. Fig. 7 second row shows the parameters of the color space change, it is a matrix multiplication that changes to opponent colors: one achromatic, and two chromatics (red-green, and yellow-blue). Fig. 7 third row shows how the normalization in the third layer accounts for a contractive function in the achromatic channel while keeping the chromatic channels unchanged. Fig. 7 fourth row shows the center-surround filters, the values for these filters have been selected in order to perform a band-pass filter according with the achromatic and chromatic CSF. Values for the parameters in layer 5 perform a spatial normalization which takes into account close neighbours. These relations

TABLE V: Initial parameters of the parametric model. All of them have been chosen to produce a behavior that resembles the visual system. **Falta hablar de f_s o la asuncion de distancia de observación como (lógicamente) hace Mantiuk el de Cambridge -aunque no es estandard y no lo hace mucha otra gente ;-). Nosotros, por lo que sea, si lo hacemos como en Cambridge.-**

Layer 1 (DN - "Luminance Normalization")			
	A	T	D
β	0.1		
H	0.5		
Layer 2 (Conv - Color)			
Jameson & Hurvich transformation			
Layer 3 (DN - "Color Normalization")			
	A	T	D
β	1	1	1
H	1/3	1/3	1/3
Layer 4 (Conv "DoG")			
	A	T	D
A	1, 0, 0	0, 1, 0	0, 0, 1
K	1.1, 1.1, 1.1	5, 5, 5	5, 5, 5
$\log\sigma$	-1.9...	-1.76...	-1.76...
Layer 5 (DN - "LGN Normalization")			
	A	T	D
A	1	1	1
β	0.1	0.1	0.1
γ	25	25	25
Layer 6 (Conv - "V1 Gabor")			
	A	T	D
f	2,4,8,16	3,6	3,6
γ_{fx}	1.87, 3.48, 6.50, 12.13	2.69, 5.02	2.69, 5.02
γ_{fy}	1.49, 2.79, 5.20, 9.70	2.15, 4.01	2.15, 4.01
θ_f	0, $\pi/8$, $2\pi/8$, $3\pi/8$, $4\pi/8$, $5\pi/8$, $6\pi/8$, $7\pi/8$		
θ_{env}	0, $\pi/8$, $2\pi/8$, $3\pi/8$, $4\pi/8$, $5\pi/8$, $6\pi/8$, $7\pi/8$		
Layer 7 (DN - "V1 Normalization")			
A	1...		
γ_s	5...		
	A	T	D
γ_f	1.25, 0.63, 0.31, 0.16	0.83, 0.42	0.83, 0.42
γ_o	0.11 π , 0.11 π , 0.11 π , 0.11 π , 0.11 π , 0.11 π , 0.11 π , 0.11 π		
B	1...		

follow a spatial Gaussian (Fig. 7 row 5), and have a saturation effect which depends on the neighbours energy (Fig. 7 row 6). Parameters for layer 6 have been chosen to have 8 equispaced orientations, 4 power-distributed scales, and independent filters for the achromatic and each chromatic channel. Since the visual system is more sensitive to achromatic than chromatic stimuli, we use half of the filters for the achromatic channel and half to both chromatic channels. The filters of the resulting transformation are shown in Fig. 9. Finally the last layer parameters were chosen to normalize the input taking into account the activity of close neighbours in frequency, orientation, and space. The parameter B is the one that determines the importance to each output channel, this parameter was fitted in all the cases to match human perception. Parameters for the last layer can be seen in Fig. 11.